BONDING BETWEEN THE CONCRETE AND FIBER REINFORCED PLASTIC (FRP) RODS

by

Wai How Soong

A Thesis
Submitted to the Faculty of Graduate Studies
In Partial Fulfillment of the Requirements
For the Degree of

MASTER OF SCIENCE

Department of Mechanical and Industrial Engineering

University of Manitoba

THE UNIVERSITY OF MANITOBA

FACULTY OF GRADUATE STUDIES

*****

COPYRIGHT PERMISSION

BONDING BETWEEN THE CONCRETE AND FIBER REINFORCED PLASTIC (FRP) RODS

BY

WAI HOW SOONG

A Thesis/Practicum submitted to the Faculty of Graduate Studies of The University of Manitoba in partial fulfillment of the requirement of the degree

of

MASTER OF SCIENCE

ABSTRACT

The bonding between the Fiber Reinforced Plastic (FRP) rods and concrete is one important factor that determines the performance of FRP reinforced concrete structure. The objective of this study is to measure the interfacial bond strength and to understand the factors that influence this. Two types of interfacial bond strength, Intrinsic Interfacial Bond Strength and Apparent Interfacial Bond Strength have been defined and measured using a single fiber pull-out test. Composite tendons with various surface profiles such as smooth, with lugs, sand coated and machined surface, were tested to study the effect of surface roughness, frictional resistance and bearing resistance on the measured intrinsic and apparent shear strength values. Loading rates were also varied to study their influence on the debond progression and on the measured apparent shear strength. Based on the experimental results following conclusions can be made:

a. Apparent bond strength between the FRP – concrete interface is attributed to bonding mechanisms such as chemical bonding, confinement pressure, frictional resistance and bearing resistance.

b. Contribution from intrinsic bonding mechanisms such as chemical bonding and confinements pressure alone is not sufficient to achieve high FRP-concrete bond strength.

c. Further improvement of the apparent bond strength can be achieved by additional mechanisms such frictional resistance and bearing resistance.

d. Apparent bond strength of sand particle coating (ISOROD^{TM}) is influenced by the loading rate due to relatively higher contribution from frictional resistance.

Acknowledgments

I would like to express my sincere gratitude to my dissertation advisor, Dr. Jayaraman Raghavan, for continued support, guidance, and help throughout this thesis, I would also like to express my gratitude to my co-advisor, Dr. Sami Rizkalla for his helpful comments and valuable suggestions in the process. In addition, I would like to gratefully acknowledge the research technician, Mr. Moray Mcvey and Mr. John Van Dorp, for their assistance and help during the experimental phase of this study.

I would also like to thank ISIS (Canadian Network Centres of Excellence for Intelligent Sensing for Innovative Structure) and University of Manitoba for the financial support for this project.

Special thanks go to all the graduate students and technicians for offering assistances in whatsoever throughout this thesis project.

Table of Content

Abstract iii

Acknowledgements v

List of Figures ix

List of Tables xi

Chapter 1
Introduction
1.1 Introduction 1
1.2 Organization of Thesis 13

Chapter 2
Literature Review
2.1 Introduction 14
2.2 FRP Reinforcement 14
2.2.1 Constituent Materials 14
2.2.2 Manufacturing 15
2.3 Testing Methods 16
2.4 Published Results on Interfacial Bond Strength 21
2.4.1 Chemical Bonding 23
2.4.2 Confinement Pressure on Bond Strength 24
2.4.3 Embeddment Length 27
2.4.4 FRP Rod Diameter 31
2.4.5 Concrete Strength 31
2.4.6 Surface Geometry of FRP Rod 33
2.5 Summary 36
2.6 Current Research Methodology 37

2.7 Thesis Objectives 41

Chapter 3

Experimental Details

3.1 Introduction 44

3.2 Specimen 44

3.2.1 FRP Reinforcement 46

3.2.2 Concrete 52

3.3 Direct Pull-out Test 54

3.4 Testing Procedure 56

3.5 Post-mortem Process 60

Chapter 4

Results and Discussion

4.1 Introduction 64

4.2 Results 65

4.2.1 Determination of Critical Embeddment Length 65

4.2.2 Determination of the Intrinsic and Apparent Interfacial Bond Strength 68

4.2.2.1 Intrinsic Interfacial Bond Strength 70

4.2.2.2 Apparent Interfacial Bond Strength 73

4.2.3 Effect of Loading Rate on Apparent Interfacial Bond Strength 97

4.3 Summary 100

Chapter 5

Conclusion and Recommendation

5.1 Conclusion 104

5.2 Recommendation 107

Reference 109

Bibliography 111
Appendix 112

List of Figures

Figure 1.1 Schematic Diagram of the Direct Pull-out Test by Boyle [9] 5
Figure 2.1 Direct Pull-out Test [8] 19
Figure 2.2 Rod-rod Pull-out Test [8] 19
Figure 2.3 Beam Test [3] 22
Figure 2.4 Load – Embeddment Length Relation in Pull-out Test 28
Figure 2.5 Schematic Load – Slip Plot for a Typical FRP Rod 43
Figure 3.1 Schematic Diagram of Specimen 45
Figure 3.2 Tested FRP Rods 48
Figure 3.3 Surface Geometry of the C-BAR™ 49
Figure 3.4 Direct Pull-out Test Setup 55
Figure 3.5 Locations of LVDTs 57
Figure 3.6 Post Mortem for Tested Sample 63
Figure 4.1a Summary of the experimental result in Part I 66
Figure 4.1b Average Apparent Bond Strength for Lugged and Machined FRP Rod 66
Figure 4.2 Load – Slip Plot for SC Specimen 69
Figure 4.3 Summary of Average Intrinsic Bond Strength 71
Figure 4.4 Summary of Average Apparent Bond Strength 75
Figure 4.5 Load – Slip Plot for MC Specimen 77
Figure 4.6 Load – Slip Plot for SCC Specimen 77
Figure 4.7 Load – Slip Plot for SLC Specimen 78
Figure 4.8a Summary of Frictional Stress 79
Figure 4.8b Summary of Frictional Stress 79
Figure 4.9a Post-mortem Examination on SC Specimen (F_a = 100%) 82
Figure 4.9b Post-mortem Examination on SC Specimen (concrete interface).....82
Figure 4.10 Post-mortem Examination on MC Specimen (F_a = 100%) 83
Figure 4.11 Post-mortem Examination on SCC Specimen (F_a = 100%) 85
Figure 4.12 Debonded (sand-particle) vs. Load 86

Figure 4.13 Average Bearing Resistance of Lugs 88
Figure 4.14 Post-mortem Examination on LC Specimen (F_a = 70%) 91
Figure 4.15 Post-mortem Examination on SLC Secimen (F_a = 100%)..... 92
Figure 4.16 Load vs. Number of Lug Fracture for Intended Specimen 93
Figure 4.17 Load – Slip Plots for Indented Specimens 96
Figure 4.18 Load – Slip Plots for SCC, MC and SC Specimen 96
Figure 4.19a Loading Rate vs. Apparent Load
Sand Coated Specimen (SCC) 98
Figure 4.19b Loading Rate vs. Apparent Load Specimen with Lugs (RLD) 98
Figure 4.20 Summary of Contribution of Bonding Mechanism to
Apparent Load 101
Figure A1 Post-mortem Examination on RLA Specimen (F_a = 100%) 120
Figure A2 Post-mortem Examination on RLB Specimen (F_a = 100%) 120
Figure A3 Post-mortem Examination on RLD Specimen (F_a = 100%).....121
Figure A4 Post-mortem Examination on RLE Specimen (F_a = 100%) 121
Figure B1 Post-mortem Examination on SCC Specimen (F_a = 100%) 122
Figure B2 Post-mortem Examination on SCC Specimen (F_a = 90%) 122
Figure B3 Post-mortem Examination on SCC Specimen (F_a = 70%) 123
Figure B4 Post-mortem Examination on SCC Specimen (F_a = 50%) 123
Figure C1 Post-mortem Examination on RLC Specimen (F_a = 85%) 124
Figure C2 Post-mortem Examination on RLC Specimen (F_a = 60%) 124
Figure D1 Post-mortem Examination on SLC Specimen (F_a = 100%) 125
Figure D2 Post-mortem Examination on SLC Specimen (F_a = 80%) 125
Figure D3 Post-mortem Examination on SLC Specimen (F_a = 60%) 126
Figure D4 Post-mortem Examination on SLC Specimen (F_a = 30%) 126
Figure E1 Post-mortem Examination on TLC Specimen (F_a = 100%) 127
Figure E2 Post-mortem Examination on TLC Specimen (F_a = 75%) 127
Figure E3 Post-mortem Examination on TLC Specimen (F_a = 50%) 128

List of Tables

Table 1.1. Summary of Published Interfacial Bond Strength Results 8
Table 1.2. Information of Surface Profile
and Mechanical Properties of the FRP Rods 9
Table 1.3. Testing Parameters of Different Researchers 10
Table 1.4. Comparison of the Results of Finding by
Two Groups of Researchers 12
Table 2.1 Comparison Between Direct Pull-out Test & Rod-rod Test [8] 20
Table 2.2 Maximum Pull-out Load and Bond Strength for Different
Curing and Testing Condition [8] 26
Table 2.3 Effect of Embeddment Length on Bond Strength 29
Table 2.4 Effect of Rod Diameter on Interfacial Bond Strength 32
Table 2.5 Effect of Concrete Strength on Interfacial
Bond Strength by Al-Zahrani 32
Table 2.6a Effects of Surface Geometries on Interfacial Bond Strength 34
Table 2.6b Effects of Surface Geometries on Interfacial Bond Strength 34
Table 3.1 Mechanical Properties of GFRP Rods [14,15] 47
Table 3.2 Various Surface Geometries of C-BAR™ 51
Table 3.3 Composition of Concrete Mixture [16] 53
Table 3.4 Summary of the Pull-out Test (Part 1) 59
Table 3.5 Summary of the Pull-out Test (Part 2 and 3) 61
Table 4.1 Summary of the Pull-out Test in Part 1 67
Table 4.2 Summaries of the Average Intrinsic Load
and Interfacial Bond Strength 72
Table 4.3 Summaries of Average Apparent Load
and Interfacial Bond Strength 74
Table 4.4 Summary of Nominal Frictional Load and Stress 80
Table 4.5 Average Bearing Resistance and Strength 89
Table 4.6 Summary of Number of Lug Fracture verses the Pull-out Load 94
Table 4.7 Results of Displacement Rate and Average Apparent Load 99

Table 4.8 Summary of Contribution of Bonding Mechanism
to Apparent Load 102
Table A Results From Direct Pull-out Test on RL-series Specimen (Test 1) ...113
Table B Results From Direct Pull-out Test on M-series Specimen (Test 1) 114
Table C Results for Measured Intrinsic Load and
Intrinsic Interfacial Bond Strength 115
Table D Results for Measured Apparent Load and
Apparent Interfacial Bond Strength 116
Table E Results for Measured Frictional Resistance and Frictional Stress 117
Table F Results for Calculated Bearing Resistance 118
Table G Results for Measured Apparent Load with
Three Different Loading Rate 119

Chapter 1

Introduction

1.1 Introduction

Advanced composite materials have long been applied in the aerospace and automotive industries because of their unique mechanical properties such as high specific strength, modulus and corrosion resistance. In the last two decades, composite materials have started to attract attention from the construction community especially for reinforcing the concrete structure.

Concrete has been the most commonly used construction materials, due to the low material cost and excellent workability. Concrete, which is a proper mixture of sand, coarse aggregate, water and cement, is a particulate composite in which both the particulate and the matrix are ceramic materials. A hydration reaction between water and the chemical substances in the cement provides a strong matrix that holds the aggregate in place. In general, like most of the ceramic-based materials, concrete can achieve excellent compressive strength. However, it has very poor tensile properties, due to the porosity and interfaces present in the brittle structure. The load bearing ability of concrete in tension can be greatly improved by introducing a reinforcement into the ceramic-based matrix. This type of concrete is usually referred as reinforced concrete. In the vast majority of the reinforced concrete used in construction application, steel

rebar (steel reinforcing bar) continues to be the most common reinforcement material. The concrete transfers the major portion of the tensile load to the reinforcing steel, which has good tensile properties. Hence, the reinforcing steel rebar enhances the load-bearing capability of the reinforced concrete under tensile loading. Despite the effectiveness and cost efficiency of the steel reinforcement materials, corrosion of reinforcing steel in the aggressive service environment leads to long-term durability problems. The corrosion of steel rebar has become the major cause of failure of concrete structures, such as deterioration of bridges and other concrete structures. The major cause of the degradation is the de-icing agents, such as salt that is applied on the bridge during winter. Poor quality of the concrete with high permeability also accelerates the corrosion of the steel reinforced concrete structure, by allowing the corrosion-inducing agents (oxygen, moisture and chloride ions) to penetrate. Billions of dollars are needed to repair or replace these aging structures [1].

Research has been pursued in the past to understand the corrosion mechanism and design solutions to the problem. Several solutions, such as anodic protection and epoxy coated steel rebar, have been explored. The idea behind the epoxy coating is to prevent the corrosive agents from reaching the surface of the steel rebar. However, it requires greater care during installation and the material and handling cost is high. This drawback has limited the application and development of these techniques to only aggressive chemical environment.

During the past decade, scientists have been focusing on non-metallic reinforcement materials, such as Fiber Reinforced Polymer (FRP), as an alternative solution to the corrosion problem in concrete structure. In general, FRP reinforcement has the following advantages over steel:

- Excellent corrosion resistance in aggressive environment
- High specific strength and modulus
- Low thermal expansion coefficient

FRP reinforcement materials consist primarily of an organic or inorganic fiber and a polymeric resin. In general, FRP reinforcement products are made of carbon, glass or aramid fibers, and epoxy / vinyl matrix. Most of these commercially available FRP reinforcements (or FRP rebars in the jargon of construction community) have various surface profiles such as ribs, lugs or indentation. The FRP reinforcement bar will be referred as FRP rod in this thesis. The function of this surface profile on the FRP rod is the same as that of the helical deformation found on the steel rebars i.e. to provide improvement in the bearing resistance to the pull-out of FRP rod.

However, high material cost is the main drawback of these FRP reinforcement materials. Another disadvantage includes low failure strain. Furthermore, FRP reinforced concrete is a relatively new concept to the construction community. Currently, construction codes and standards for reinforcing concrete are primarily

for steel reinforced concrete. Well-established construction codes and design standards on FRP reinforced concrete are not available. This, as well as a lack of knowledge on the performance of FRP reinforced concrete, has limited its application. When compared to steel reinforcement, FRP reinforcement has anisotropic properties, its shear and transverse properties are controlled by the properties of resin and longitudinal properties are controlled by the reinforcing fiber. In general, it has a lower failure strain. Thus, load transfer from the concrete to the FRP rod is very different than to the steel rebar.

In order to establish a design code and construction standard for the FRP reinforcement concrete, bonding between the FRP rod and the concrete needs to be understood and quantified. Currently, there is no standardized testing method for determining the interfacial bond strength between the FRP reinforcement and concrete. Research studies to understand the bonding between the FRP reinforcement and concrete have been carried out by a number of researchers [2,3,4,5,6,7,8,9] in the past. One of the most widely used testing method to measure the interfacial bond strength between FRP reinforcement and concrete is the direct fiber pull-out test [2,5,6,7,8,9]. A schematic diagram of the direct pull-out test is shown in the Figure 1.1. The FRP reinforcement embedded in a concrete block or concrete cylinder is subjected to a tensile pull-out load and the pull-out load is measured. The relative movement or slip between FRP rod and concrete at both the load-end and free-end of the specimen is normally measured by a LVDT (linear variable displacement transducer) while the load is

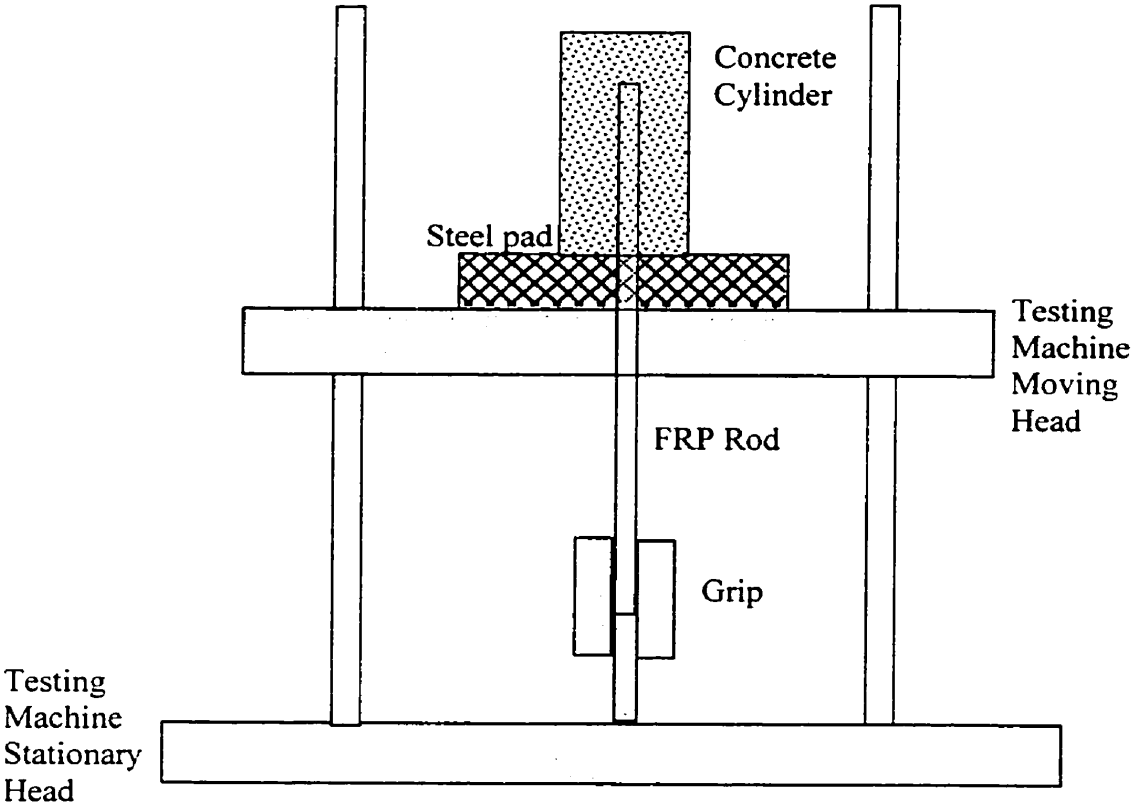

Figure 1.1 Schematic diagram of the direct pull-out test by Boyle [9]

applied to the FRP rod. Several other types of testing methods have been developed as well, such as the beam test [3] and rod-rod pull-out test [8]. The detail of these different testing methods will be discussed in the Chapter 2.

Generally, the Interfacial bond strength τ (also referred as interfacial shear strength) is defined by equation 1.1.

$$\tau = \frac{P_{max}}{A} \qquad (1.1)$$

Where P_{max} is the maximum pull-out load and A is the contact area between the FRP reinforcement and concrete. This interfacial bond strength should be referred as the average interfacial bond strength since the shear stress is assumed to be constant along the embedded FRP reinforcement. However, in reality the shear stress varies along the embedded FRP rod [4,8,10,11]. The actual interfacial bond strength is difficult to measure unless the stress distribution along the embedded region of the FRP reinforcement is accurately known. The concept of the nominal interfacial bond has been widely accepted. Accordingly, interfacial bond strength reported in this thesis is also the average interfacial bond strength.

A summary of published results for interfacial bond strength is given in Table 1.1. Properties and dimensions of FRP reinforcement as well as testing conditions,

are used to obtain the results, are tabulated in Table 1.1 are given in Table 1.2 and 1.3 respectively. In general, the FRP used in these studies were either glass fiber reinforced epoxy or carbon fiber reinforced epoxy and both FRP had similar modulus. The concrete used by the research groups also had similar strength except that of Tighouart et al. [3]. Despite this, the reported interfacial bond strength varied by a wide margin from one research group to another as well as within the findings of a research group.

Results from all the research groups indicate that the measured interfacial bond strength decreases with an increase in FRP rod diameter. Results from Benmokrane et al. [7] and Freimanis et al. [2] indicate that, the interfacial bond strength varied with lug dimensions, for a given diameter and embedment length of the FRP rod. Al-Zahrani's [8] results indicate that the presence or absence of lugs can have a major influence on the measured interfacial bond strength. It can also be inferred from the results of Tighouart et al. [3], that the shape of deformation (lugs or helical wraps) on the surface of the FRP can have significant influence on the measured interfacial bond strength.

Finally, to illustrate the influence of loading rate and inconsistency in the definition of contact area (specifically between the concrete and the FRP with surface deformation), the measured maximum pull-out load and calculated interfacial bond strength from two researchers are compared in Table 1.4. Despite having the same diameter and embedment length, the loading rate used

Table 1.1. Summary of Published Interfacial Bond Strength Results

Author	Types of FRP	Nominal Rod Diameter (mm)	Embeddment Length (mm)	Interfacial Bond Strength (MPa)
Benmokrane et al. [7]	C-BAR™ (P1)	12.7	63.5	18.4
	C-BAR™ (P1)	12.7	127.0	14.5
	C-BAR™ (P2)	12.5	63.5	16.8
	H. B. Rebar	12.5	63.5	15.1
	H. B. Rebar	12.5	127.0	12.7
Al-Zahrani [8]	Machined GFRP	12.7	63.5	39.7
	Machined GFRP	12.7	127.0	29.7
	Smooth GRFP	6.35	63.5	1.37
	Smooth GFRP	12.7	63.5	0.97
Tighiouart et al [3]	GRFP (Type A)	12.7	127.0	10.6
		15.9	127.0	7.3
		19.1	127.0	6.6
		25.4	127.0	6.4
	GFRP (Type B)	12.7	127.0	12.3
		15.9	127.0	10.8
		19.1	127.0	--
		25.4	127.0	7.4
Freimanis et al [2]	H. B. Rebar a	12.7	63.5	7.8
	H. B. Rebar b	12.7	63.5	16.0
	H. B. Rebar c	12.7	63.5	9.8
	H. B. Rebar d	12.7	63.5	17.2
	H. B. Rebar e	12.7	63.5	18.2
	H. B. Rebar f	12.7	63.5	14.4

Table 1.2. Information of Surface Profile and Mechanical Properties of the FRP Rods

Reference	Type of FRP Rod	Surface Profile of the FRP Rod	Lug Dimension Depth x Width mm	Nominal Ultimate Tensile Strength MPa	Modulus of Elasticity GPa
Benmokrane et al. [7]	C-BAR™ (P1)	Lugged Surface	1.3 x 2.8	736	42
	C-BAR™ (P2)	Lugged Surface	0.9 x 3.5	743	40
Al-Zahrani [8]	Machined GFRP	Lugged Surface	1.3 x 3.8	N.A	42
	Smooth GRFP	Smooth Surface	N.A	N.A	40
Tighiouart et al. [3]	GRFP (Type A)	Deformed Surface with Helical Winding	N.A	683	42
	GFRP (Type B)	Resin Impregnated Strand Wrapping	N.A	690	42
Freimanis et al. [2]	H. B. Rebar a	Helical Wrap with silica sand particle coating	0.381 x 22.2*	690	37
	H. B. Rebar b		0.381 x 31.8*	610	35
	H. B. Rebar c		0.381 x 38.1*	690	38
	H. B. Rebar d		0.889 x 22.2*	570	35
	H. B. Rebar e		0.889 x 31.8*	530	36
	H. B. Rebar f		0.889 x 38.1*	510	40

* Note : Pitch Length (mm)

Table 1.3. Testing Parameters of Different Researchers

Reference	**Type of Testing**	**Nominal Strength of concrete** **MPa**	**Note**
Benmokrane et al. [7]	Direct Pull-out Test	45	Loading Rate = 22 kN / min Normal Concrete
Al-Zahrani [8]	Direct Pull-out Test	45	Displacement control = 0.125 mm / min High Early Strength Concrete (14-day curing)
Tighiouart et al. [3]	Beam Test	31	N.A
Freimanis et al. [2]	Direct Pull-out Test	45	Displacement control = 1.25 mm/min

by the former was different from that of this latter. This appears to be the reason for the difference in the maximum pull-out load.

Moreover, Al-Zahrani reported a bond strength higher then that reported by Benmokrane et al. [7], despite a lower pull-out load and similar dimensions. This apparent discrepancy can be attributed to the difference in the definition and thus calculation of the contact area between the two groups of researchers. Benmokrane et al. [7] calculated the contact area using an average diameter of the FRP rod. However, Al-Zahrani [8] calculated the contact area using the lug dimensions and the diameter of the rod.

The interfacial bond strength is dependent only on chemical bonding between the FRP and the concrete. Thus it should not be dependent on the test parameters discussed above. However, the variation in the published interfacial bond strength with test parameters suggest that mechanisms other than the chemical bonding have significant influence on the measured interfacial strength. These mechanisms have to be delineated and the influences of test parameter on each of the mechanisms have been quantified, in order to understand the observed variation in Table 1.1. Moreover, the development of a standard test method and test parameter is not possible unless this knowledge is developed. Hence this thesis is focused on (a) developing a comprehensive understanding of the various mechanisms that contribute to the measured interfacial bond strength

Table 1.4. Comparison of the Results of Finding by Two Groups of Researchers

Reference	**Types of FRP**	**Nominal Lug Dimension** **Depth x Width** **mm**	**Nominal Rod Diameter** **mm**	**Loading / Displacement Rate**	**Max. Pull-out Load** **kN**	**Interfacial Bond Strength** **MPa**
Benmokrane et al. [7]	C-BAR™ (P1) Commercial Available GFRP Rod	1.3 x 2.8	12.7	22 kN/ min	46.0	18.4
Al-Zahrani [8]	Machined GFRP Rod	1.3 x 3.8	12.7	0.125 mm/min	24.2	39.7

and (b) understanding the influences of test parameter on the contribution of each of the mechanisms identified in (a).

Two Types of interfacial bond strength are defined and measured: (i) intrinsic bond strength dependent on chemical bonding, and misfit strain due to CTE (Coefficient of Thermal Expansion) mismatch between FRP and concrete, and concrete cure shrinkage; (ii) apparent bond strength dependent on intrinsic bond strength and other mechanisms such as bearing resistance and frictional resistance. Contributions of each of these mechanisms to the measured apparent bond strength and their dependence on various test parameters are studied and quantified.

1.2 Organization of Thesis

Published literature on interfacial bond strength is presented and carefully reviewed in Chapter 2. The objective of this thesis, formulated based on the published literature is presented at the end of Chapter 2. The experimental details are presented in Chapter 3. The results of this experimental work are presented and discussed in Chapter 4. Finally, conclusions based on experimental results are presented in Chapter 5. Results from individual experiment and additional figures from post-mortem examination are given in appendix.

Chapter 2

Literature Review

2.1 Introduction

This literature review starts with a brief introduction on the constituent materials and manufacturing methods of the fiber-reinforced polymer (FRP) rebars. Following this, a brief review of the testing methods for determining the interfacial bond strength between the FRP rods and concrete is presented. Subsequently, a review and discussion of the published research results are presented. The objectives of the thesis are presented at the end of this chapter.

2.2 FRP Reinforcement

2.2.1 Constituent Materials

Fibers and matrices are the two main constituents of a FRP rod used as concrete reinforcement. Generally, a fiber has the unique mechanical properties such as high specific stiffness and strength. Matrices, on other hand, are relatively more ductile when compared to the fiber and act as a binding and protection medium for the fibers. The most important role for the matrices is to assist the load transfer from the reinforced concrete to the fibers. Fibers can be categorized into two main groups, as organic and inorganic fibers. These two types of fiber

products are commercially available. Carbon, aramid and PVA (Poly vinyl alcohol) are the common organic fibers. On the other hand, glass (E, S and A-glass) fibers are the most common inorganic fibers. Thus, based on the types of fiber, FRP reinforcement products can be referred as carbon fiber reinforced polymer (CFRP), glass fiber reinforced polymer (GFRP) and aramid-reinforced polymer (AFRP). Thermoset resins such as epoxy, polyester and vinyl ester are most widely used as a matrix in FRP reinforcements. The reasons are better processibility and lower cost when compared to thermoplastic resins.

The performance of the FRP rebars is greatly dependent on the type of fiber and matrix, and shape of the rebars. Furthermore, it is also dependent on the volume fraction of the fiber in the FRP reinforcement. In general, commercially available FRP products are manufactured to its highest fiber content (60% - 70%) allowable by the manufacturing method.

2.2.2 Manufacturing

Researchers have tested different types of FRP rod and most of them are commercial available GFRP rod such as C-BAR^{TM} and Hughes Brother (H.B.) Rebar. These FRP rods differ in their surface geometry.

The pultrusion method is the most commonly used manufacturing method for fabricating FRP rods. By combining pultrusion and filament winding, rebar with different surface geometries are manufactured. Helical wrapping or coiling is the

common surface geometry found on the commercial FRP rebars such as Hughes Brother Rebar, which is similar to the surface geometry of steel rebars. The bearing resistance to the pull-out of the reinforcement from the concrete can be enhanced by these surface geometries of the FRP rods. Braiding or continuous lamination is another technique that has been accepted by the manufacturers. By coating the final product of FRP materials with a layer of silica particles, the pull-out load has also been altered in FRP rods such as the sand-coated ISOROD™ and the H.B. Rebar. Other types of deformation such as depression or indentation, that serve the same purpose, are obtained by pressing the pultruted FRP rod to form lugs on the surface of the FRP rod before the resin hardens. This technique is used in fabricating the FRP rod such as C-BAR™.

2.3 Testing Methods

Currently, there is no standardized test method available to determine the bond strength between the FRP rebar and the concrete. The testing methods and models, which are based on experience with conventional steel reinforced concrete system, are currently being extended to FRP reinforced concrete. The American Society for Testing and Materials (ASTM) has developed a standard concentric / direct pull-out test (ASTM C234) for the comparison of different concrete mixtures. Though this method has not been developed for assessing the interfacial bond strength, it has become the most popular test method among researchers [2,5,6,7,8,9].

As shown in the Figure 2.1, a cylindrical concrete specimen with an embedded FRP rod is used. The FRP rod is pulled out of the concrete specimens under a tensile load. The relative displacement of the FRP rod with respect to the concrete at both the load and free ends, which is referred as load and free-end slip in the thesis respectively, is also measured. This applied load increases until a maximum load when FRP pulls out of the concrete. The interfacial bond strength is measured using the maximum pull-out load and contact area as shown in equation 1.1.

The direct pull-out test offers the advantage of simplicity for measuring interfacial bond strength for the FRP reinforced concrete. However, it also has two disadvantages:

- The concrete is subjected to a compression load at the loading surface
- The concrete surrounding the FRP reinforcing rod has a tendency to split

To over come the concrete splitting problem found in the direct pull-out test, a confining reinforcement is used. Better concrete confinement can be provided by restricting the embedded area several inches away from the loading surface [7,8]. The restraining length between the embeddment region and the concrete surface is referred as debonded length, which is shown in Figure 2.1.

Another method to remove compression on the concrete face, which is shown in Figure 2.2, is the rod-rod pull-out test. In this case, the specimen consists of a concrete prismatic sample, with two reinforcement rods embedded at opposite ends. The two rods have different embeddment lengths so that pull-out is restricted to the shorter one. The load and slip at the loaded end are measured similar to the direct pull-out test. The disadvantage of this type of pull-out test is the inability to measure the free-end slip directly.

Al-Zahrani [8] had conducted experiments to compare the results from direct and rod-rod pull-out test with same embeddment length and FRP rod diameter. The results are tabulated Table 2.1, similar values for the maximum pull-out load obtained from both test methods suggest that the compressive stress field in the concrete near the load end did not affect the results obtained using direct pull-out test. Confining the bonded region to the interior of the concrete by using a 'bond breaker' at both ends (to debond the FRP from the concrete), prevented the splitting of the concrete was not observed at the load end during direct pull-out test.

One shortcoming of both the direct and rod-rod pull-out tests, is their inability to reproduce the stress field in a reinforced concrete beam under a bending load, a common service condition for reinforced concrete. A beam test has been developed for this purpose.

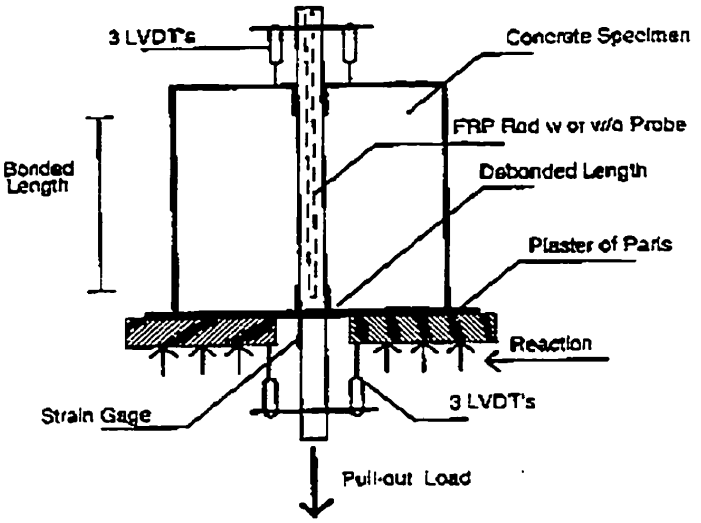

Figure 2.1 Direct Pull-out Test [8]

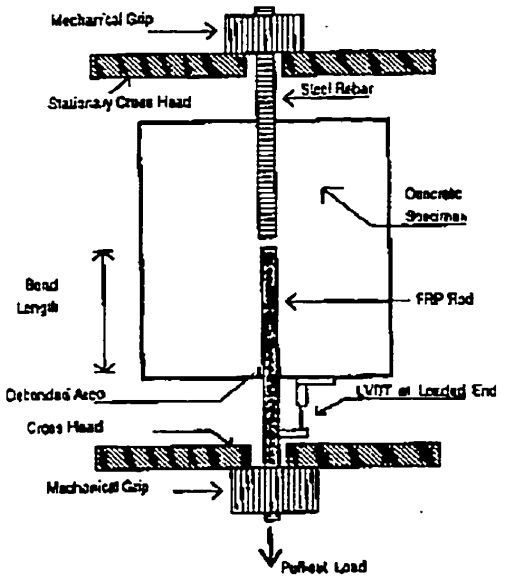

Figure 2.2 Rod-rod Pull-out Test [8]

Table 2.1 Comparison Between Direct Pull-out Test & Rod-rod Test [8]

Specimen	**Direct Pull-out Test**	**Rod-rod Test**
	Average Maximum Load (N)	
Smooth GFRP	3881 ± 4.79	4032 ± 10.72
Machined GFRP	23187 ± 4.48	24169 ± 1.11

The specimen consists of two rectangular blocks of reinforced concrete that are coupled by a hinge at the top and are joined by FRP reinforcement at the bottom, as illustrated in Figure 2.3. The beam is loaded in bending by two equal forces applied symmetrically on either side of the hinges. The slips at the free ends of the reinforcing rod are measured. Though the beam test represents the actual stress field more closely when compared to direct pull-out test, the testing procedure is relatively more complex.

2.4 Published Results on Interfacial Bond Strength

Considerable amount of research have been conducted on quantifying the interfacial bonding between FRP rod and concrete. Experiments were conducted on FRP rod with different embeddment length, diameter, surface geometry and testing condition. A summary of the results is given in Table 1.1 and Table 1.3. The various parameters, which affect the interfacial bond strength, have been studied are:

- Chemical Bonding
- Confinement Pressure
- Embeddment length
- FRP rod diameter
- FRP rod diameter
- Compressive strength of concrete
- Surface geometry of the FRP rod

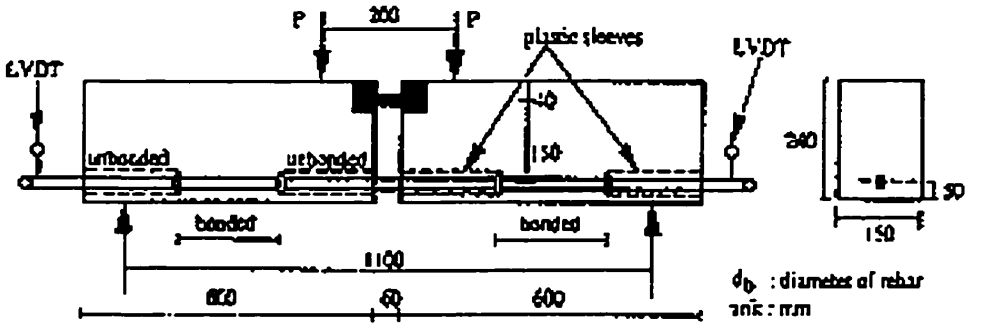

Figure 2.3 Beam Test [3]

2.4.1 Chemical Bonding and Interfacial Microstructure

The contribution of the chemical bonding to FRP – concrete bond strength requires an investigation of a smooth FRP rod. However, most of the previous research focused on FRP rods with different surface profiles, which precluded the delineation of the contribution from chemical bonding. In general, the chemical bonding between FRP and concrete is relatively weak. Findings by Al-Zahrani [8] indicate that the bond strength between a smooth FRP rod and concrete is minimal, as shown in Table 2.2 (test 4). The measured bond strength will correspond to interfacial bond strength only if the debonding progresses along the interface region. If the region adjacent to the interface is weaker than the interfacial bond strength, this region will fracture instead of the former. The measured bond strength will not be equal to the interfacial bond strength. In order to understand the influence of region adjacent to interface, studies on the microstructure at the interface have been done by several researchers [7,12] using SEM (scanning electron microscope). Findings by Chan et al. [12] and Benmokrane et al. [7] had shown that a relatively higher concentration of CH crystal (a by-product of cement hydration) in a thin layer at the interface between FRP and concrete when compared to the microstructure of the bulk cement. Chan et al. [12] had indicated that the higher concentration of CH crystal layer, which had a higher porosity, resulted a transition zone (interphase) with less density. This type of transition zone had also been found in the steel rebar – concrete interface [13]. This porous transition zone may provide an easy path for

crack propagation. Hence, the bond failure during a pull-out test may occur in this transition zone instead of failure along the interface between FRP and concrete. This type of failure is referred as cohesive type. Thus, it may influence the measured bond strength. However, this porous transition zone may not influence the bond strength, if the bond failure is an adhesive type, when the debonding occurs at the FRP – concrete interface. Thus, bond strength may be affected by the microstructure of the FRP – concrete transition zone. However, the effect of this transition zone on the bond strength of the FRP – concrete has not been quantified yet.

2.4.2 Confinement Pressure on Bond Strength

Benmokrane et al. [7] suggested that the bonding between FRP rod and concrete is due to a lateral stress or confinement pressure on the FRP rod caused by dry-shrinkage during the curing of the concrete. In addition, the epoxy resin, which acts as a binder in the FRP rod, has a tendency to absorb moisture from its surroundings. The swelling effect of the epoxy matrix due to the moisture absorption may also contribute to the additional lateral stresses acting at the FRP – concrete interface. Concrete dry-shrinkage during the hydration process is primarily affected by the water / cement ratio of the concrete mixture. In general, the amount of dry-shrinkage is directly proportional to the water / cement ratio. Yet, by altering the water / cement ratio, the compressive strength of the

concrete will be affected as well. However, a direct study of the effect of water / cement ratio on interfacial bond strength of FRP rod has not been conducted yet.

Investigation of the effect of this confinement pressure on the bond strength on the smooth GRP rod was carried out indirectly by Al-Zahrani [8]. Since, FRP rod has a higher thermal coefficient than the concrete, the effect of uniform radial pressure on the rod and consequently on the bond stress was studied by varying the curing, and testing temperature, as shown in Table 2.2.

The results for Test 1 and 2 show that a $T_t < T_c$ resulted in a lower pull-out load and bond strength than the reference data at room temperature (obtained from Test 4). This is caused by the loss of confinement pressure due to the contraction of the FRP rod at the lower test temperature. The maximum pull-out load and bond strength increased in Test 3 because of the expansion of the FRP rod at higher temperature when compared to Test 4. In the case of smooth FRP rod, the confinement pressure dominates the bond strength. Thus, the findings of Al-Zahrani [8] had proven the role of confinement pressure on interfacial bond strength. With an increase in the confinement pressure of the concrete on FRP rod, interfacial bond strength increases.

Table 2.2 Maximum Pull-out Load and Bond Strength for Different Curing and Testing Condition [8]

Test	Curing Temperature T_c °C	Testing Temperature T_t °C	Max. Pull-out Load kN	Interfacial Bond Strength MPa
1	60	20	<200	<0.04
2	20	-20	<200	<0.04
3	20	60	9053	1.79
4	20	20	4211	0.831

2.4.3 Embeddment Length:

The embeddment length of the FRP rod in the concrete has to be equal or less than the critical embeddment length (or development length in the jargon of construction community) to measure the interfacial bond strength using the direct pull-out test. Optimum embeddment length as defined by the construction community is the minimum embeddment length required for the FRP rod to carry the maximum possible load. The relationship between the applied load to pull out an embedded FRP rod from concrete and the embeddment length is shown schematically in Figure 2.4. The pull-out load will increase linearly with embeddment length until it reaches a maximum value and the embeddment length corresponding to this maximum load is the critical embeddment length (L_c). If the embeddment length is less than the critical length L_c, FRP rod will be pulled out from the concrete; FRP rod will fracture if the embeddment length is greater than critical embeddment length (L_c).

Experimental results on the effect of embeddment length on measured bond strength are tabulated in Table 2.3. Two embeddment lengths were 5 and 10 times the rod diameter. The findings in Table 2.3 show that the bond strength decreases with increase in embeddment length. Ideally, bond strength should not vary with embeddment length or rod diameter. However, Al-Zahrani's [8] results

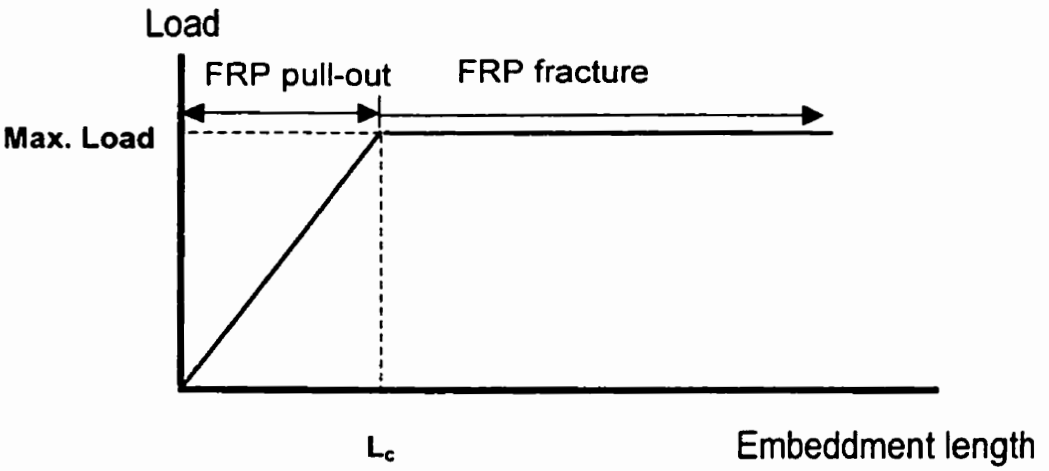

Figure 2.4 Load – Embeddment Length Relation in Pull-out Test

Table 2.3 Effect of Embeddment Length on Bond Strength

Type of FRP Rod	Rod Diameter mm	Embeddment Length mm	Nominal Bond Strength MPa	Reference
C-BAR™ (P1)	12.7	63.5	18.4	Benmokrane et al. [7]
	12.7	127.0	14.5	
H. B. Rebar	12.5	63.5	15.1	Benmokrane et al. [7]
	12.5	127.0	12.7	
Machined GFRP	12.7	63.5	39.7	Al-Zahrani [8]
	12.7	127.0	29.7	

indicates that the bond strength decreases with increase in FRP diameter even for smooth FRP rod. This can be explained using non-uniform stress load distribution along the embedded FRP rod in concrete. Al-Zahrani [8] had measured the strain field along the embeddment length of FRP rod using strain gauges. The results showed that maximum load occurred near the load-end of the FRP rod and gradually decreased to zero near the free-end. The load and stress distribution along the embeddment length varied with increase in load. This stress distribution also varied with embeddment length. However, while calculating the interfacial bond strength, a constant shear stress / force distribution was assumed. This may be the reason for variation of bond strength with increase in embeddment length.

In the case of FRP with lugs, the lugs near the load-end failed first with further increased in load, progressive failure of lugs occurred from the load - end to free – end. While this may alter the stress distribution in a complex manner, the assumption of constant force / shear stress distribution is thought to be the reason for the decrease in bond strength with increase in embeddment length.

Even though the load distribution along the FRP rod inside concrete has been studied [8], the relation between the pull-out load and the lug or rib failure on the deformed FRP rod such as C-BAR^{TM} and H.B rebar is not known at this time. Further investigation is needed to understand the relation between the lug or rib failure progression and load distribution along the embeddment length.

2.4.4 FRP Rod Diameter

Results of Tighouart et al. [3] and Al-Zahrani [8] are tabulated in Table 2.4, suggest that the nominal bond strength of the FRP rods decreases as the diameter of the FRP rod increase. Tighouart et al. [3] reasoned this to be due to bleeding of water in concrete. That is, the larger the diameter of the FRP rod, the higher the quantity of water that gets trapped in the vicinity of the FRP rod, and leads to higher amount void. This also leads to a reduction in strength since the void reduces the contact surface between the rod and concrete. The stress distribution along the embeddment length, as discussed in 2.4.3, may also be another reason.

2.4.5 Concrete Strength

Al-Zahrani [8] had conducted the direct pull-out test on the machined FRP rod, which embedded in normal concrete with average compressive strength of 31.4, 44.9, 55.2 and 66.1 MPa. The results are tabulated in Table 2.5. The measured bond strength did not vary with concrete compressive strength, and the FRP pull-out occurred by shearing of lugs on the FRP rod. Thus, he concluded that the interfacial bond strength should be independent of the compressive strength of concrete as long as the failure mode did not occur by concrete crushing between the lugs. Bond failure of the machined FRP rods also not controlled by the failure

Table 2.4 Effect of Rod Diameter on Interfacial Bond Strength

Type of FRP Rod	Nominal Rod Diameter mm	Embeddment Length mm	Nominal Bond Strength MPa	Reference
Type A	12.7	127	10.6	Tighouart et al. [3]
	15.9	127	7.3	
	19.1	127	6.6	
	25.4	127	6.4	
Type B	12.7	127	12.3	Tighouart et al. [3]
	15.9	127	10.8	
	19.1	127	--	
	25.4	127	7.4	
Smooth GFRP	6.35	63.5	1.37	Al-Zahrani [8]
	12.7	63.5	0.97	

Table 2.5 Effect of Concrete Strength on Interfacial Bond Strength by Al-Zahrani [8]

Nominal Concrete Strength MPa	Embeddment Length mm	Interfacial Bond Strength MPa
31.4	12.7	40
44.9	12.7	40
55.2	12.7	40
66.1	12.7	42

2.4.6 Surface Geometry of FRP Rod:

Strength of the concrete provided that there was enough debonded length at the load-end to avoid concrete splitting.

In general, interfacial bond strength between the FRP rod and concrete is sensitive to the surface geometry of FRP rod, as illustrated in Table 2.6a and 2.6b. Interfacial bond strength varied widely with surface geometry.

The interfacial bond strength of smooth GRFP is insignificant when compared to FRP rod with other types of surface geometry. The weak bond strength was explained to be result of weak chemical bonding [12, 13] and low frictional resistance [8]. Thus, smooth FRP rod is impractical in construction application due to the weak interfacial bond strength. One approach to improve the bonding between FRP reinforcement rod and concrete is to improve the bearing resistance through indentation or helical wrapping of the FRP surface. Such surface geometries can be found on the commercial available FRP rods such as C-BAR™, which is similar to those found on steel rebars. In addition, adhesion and friction-enhancing agents such as fine sand particles are sometimes added to the resin rich layer of material on the surface of the FRP rod to further enhance the frictional resistance. Commercially available ISOROD™ and Hughes Brother Rebar are of this type.

Table 2.6a Effects of Surface Geometries on Interfacial Bond Strength

Reference	Type of FRP Rod	Description	Lug width mm	Lug Depth mm	Bond Strength MPa
Al-Zahrani [8]	Smooth GFRP	Smooth	--	--	0.97
	Machined GFRP	Lug	3.8	1.3	39.7
	Machined GFRP	Lug	8.9	1.3	23.2
Benmokrane et al. [7]	C-BAR (P1)	Lug	2.8	1.3	18.4
Note: Embeddment Length = 63.5 mm; Rod Diameter = 12.7 mm					

Table 2.6b Effects of Surface Geometries on Interfacial Bond Strength

Reference	Type of FRP Rod	Description	Pitch length mm	Lug Depth mm	Bond Strength MPa
Freimanis et al. [2]	H. B. a Rebar	Helical Wrap with silica sand particle coating	22.2	0.381	7.8
	H. B. b Rebar		31.8	0.381	16.0
	H. B. c Rebar		38.1	0.381	9.8
	H. B. d Rebar		22.2	0.889	17.2
	H. B. e Rebar		31.8	0.889	18.2
	H. B. f Rebar		38.1	0.889	14.4
Note: Embeddment Length = 63.5 mm; Rod Diameter = 12.7 mm					

Al-Zahrani [8] has shown that the failure can change from lug shear to concrete failure when the area of the concrete between the lugs is decreased by increasing the width of the lugs on the FRP rod. Hence, the dimensions of the length of the lug and lug pitch play an important role in determining the failure mode. If the fracture mode is lug shearing, the maximum bearing resistance is limited by the shear strength of the lug. However, if the fracture mode is due to concrete failure, the bearing resistance and the pull-out load will be dependent on concrete strength.

Freimanis et al. [2] studied the effect of surface geometry of the rod on the bond strength. The tested FRP rods had helical wrapping surface deformation on the rod surface with additional sand particle coating. The findings corroborated the above findings by Al-Zahrani [8] that the bond strength could be altered with different width and depth of lugs. They tested the H.B. rebars with two different lug depths and three different pitch lengths as tabulated in Table 2.6b. All the samples had the same embeddment length and rod diameter (Table 1.4). The H. B. rebar, which had the lug with dimension of 31.8 mm x 0.889 mm (width x depth), resulted in the maximum bond strength. In addition to the bearing resistance of the lug on the rod surface, the sand particles also enhance the bond strength by providing additional frictional resistance.

Thus, the frictional and bearing resistance depend on several factors such as the surface pattern of the rod, dimensions and pitch of the lug, shear strength of the lugs, and concrete strength.

2.5 Summary

Based on the literature review, the following can be summarized:

- The published interfacial bond strength does not correspond to the stress when FRP debonds from the concrete. It corresponds to a stress when the fiber starts to pull out due to failure of lugs / wrappings, which occurs at a stress level much higher than stress levels at which debonding occurs.

- Though researchers have identified various mechanisms (such as chemical bonding, bearing resistance and frictional resistance) that contribute to the measured interfacial bond strength, these contributions have not been quantified.

- Due to lack of such delineation, factors that influence these mechanisms have not been clearly understood

- Without such delineation and understanding, arbitrary variation of various test parameters by previous researchers, resulted in a wide scatter in the published results for the interfacial bond strength.

Hence the thesis is focused on alleviating the above mentioned deficiencies in the existing literature.

2.6 Current Research Methodology

If the interfacial bond strength is dependent only on chemical bonding between the FRP and the concrete, then it should be independent on the test parameters, used by previous researchers. However, the variation of published bond strength with test parameters suggest that mechanisms other than chemical bonding have significant influence on the measured interfacial bond strength.

As discussed in section 2.4, the published interfacial strength does not correspond to intrinsic interfacial bond strength when the FRP debonds from the concrete. Hence determining the intrinsic interfacial bond strength is the first step of the research. Accordingly, the load corresponding to the complete debonding of the FRP from the concrete is defined as the intrinsic load. The mechanisms that contribute to this load are chemical bonding and lateral confinement pressure exerted by the surrounding concrete on the FRP. The parameters that influence these mechanisms are FRP material, concrete mixture and curing

conditions. These functions are referred to as intrinsic parameters since they do not change during testing. These mechanisms do not influence the intrinsic load at which FRP debonds from the concrete. The interfacial bond strength determined using intrinsic load (F_i) is defined as the intrinsic interfacial bond strength and is calculated using equation 2.1

$$\tau_i = \frac{F_i}{Area} \qquad (2.1)$$

The maximum pull-out load is defined as the apparent load (F_a). The difference between F_a and F_i corresponds to load increase caused by mechanism such as bearing resistance and frictional resistance. These mechanisms do not influence the intrinsic load at which FRP debonds from the concrete. Hence the parameters that influence these mechanisms are referred as extrinsic parameters. These parameters include loading rate, surface geometry of FRP rods and surface roughness. The interfacial bond strength determined using this apparent load is defined as the apparent interfacial bond strength and is calculated using equation 2.2.

$$\tau_a = \frac{F_a}{Area} \qquad (2.2)$$

The apparent load can be written as equation 2.3.

$$F_a = F_i + F_f + F_b. \qquad (2.3)$$

where F_f = Frictional resistance

F_b = Bearing resistance.

Apparent and intrinsic bond strength can be measured directly from a typical load - slip behavior of the direct pull-out test, which is shown in Figure 2.5. The two curves represent the load – slip relation for load-end and free-end. The displacement at both ends is a relative movement between the FRP rod and concrete when the FRP rod is subjected to a pullout load. This relative displacement is referred as slip in this thesis and is measured by the LVDTs. The load versus slip plot at the load-end can be divided into three regions. In region I, the debonding between FRP and concrete begins and ends. When the debonding progresses along the entire interface between the FRP and concrete, the free end begins to slip. The load, where the debonding has completed, i.e. where the free end starts to move, is taken to be the intrinsic load. The intrinsic interfacial bond strength can be measured as intrinsic load (F_i) divided by the total contact area of the FRP reinforcement in the concrete using equation 2.1. Because of experimental difficulties, the exact load at which the debonding starts could not be measured. Hence, the load at which debonding is completed is taken to be the intrinsic load in this thesis. The method to measure the contact

area, which is used to calculate the subsequent bond strength, will be discussed in Chapter 3.

In region II, the load continues to increase due to the frictional and bearing resistance, which is caused by the roughness or lugs on the surface of the FRP. The pull-out load continues to increase up to a value when the frictional and bearing resistance are over come by the pull-out load and the FRP rod starts to pull-out. Apparent interfacial bond strength can be determined using this maximum pull-out load, referred as apparent load (F_a) in the thesis, and the contact surfaced area between FRP rod and concrete using equation 2.2

The pull-out region after maximum load is referred as region III. The load drop in region III after the maximum load can be gradual or sharp depending on the FRP rod surface geometry. The frictional load (F_f) is defined as the load value to which the load drops as shown in Figure 2.5. Thus, the bond strength corresponding to this frictional load is defined as frictional stress (τ_f). Bearing resistance can be determined from equations 2.3. Intrinsic, frictional and apparent loads are measured from the direct pull-out test.

Once the contribution of various mechanisms such as chemical bonding, frictional resistance and bearing resistance are measured. The factors that influence each of these mechanisms can be identified and their influence

quantified. The research methodology as discussed above is expected to help in:

a. better design of FRP rod.
b. understanding the bonding between FRP and concrete
c. better design of test parameters and test method

Hence, the goals of this thesis as defined in the next section are to measure and study the contribution of various mechanisms to the apparent interfacial bond strength and the influence of various factors that affect these mechanisms. Details on testing procedure and measurement for these bonding mechanisms will be discussed in Chapter 3.

2.7 Thesis Objectives

Based on the literature review, the following objectives have been formulated for this thesis.

- Design a research methodology to define the contributions of various mechanisms that contribute to the interfacial bond strength.

- Measure the intrinsic and apparent interfacial bond strength using the direct fiber pull-out test.

- Study the factors that influence both the intrinsic and apparent interfacial bond strength and quantify their influence.

- Develop a prediction model to predict the apparent interfacial bond strength.

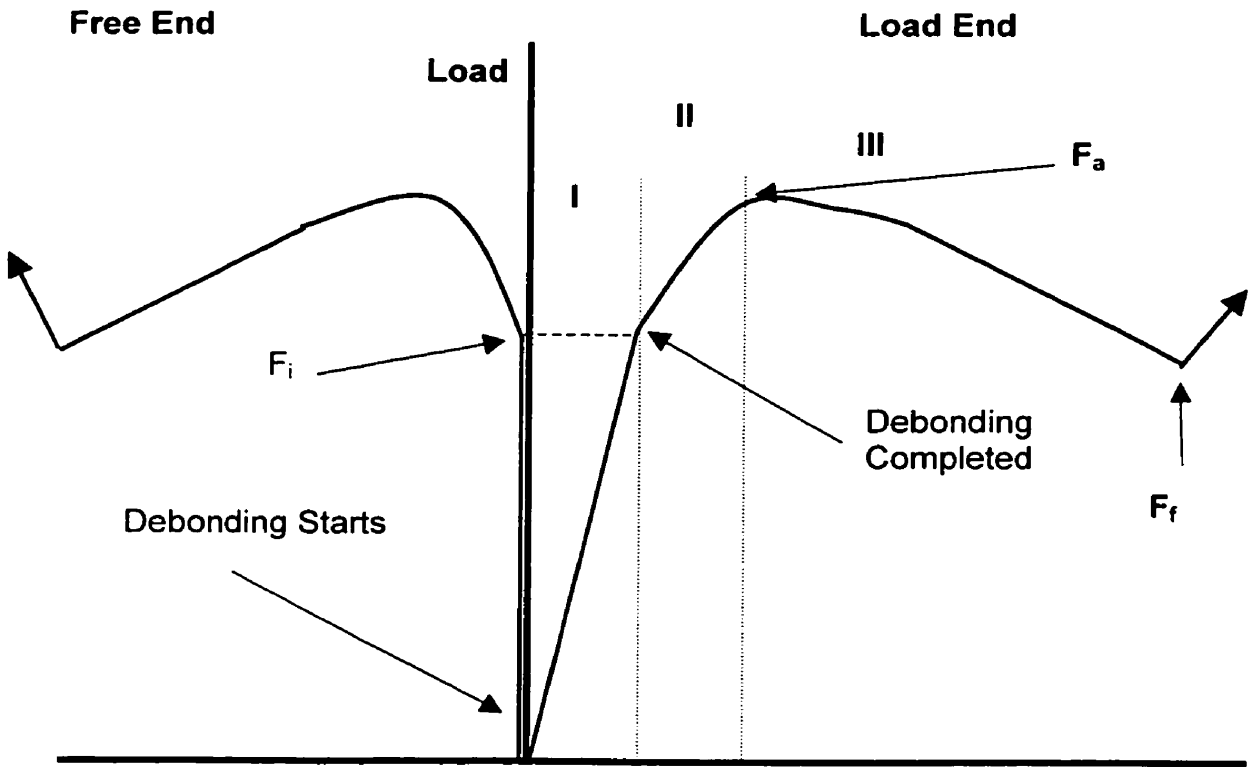

Figure 2.5 Schematic Load – Slip Plot for a Typical FRP Rod

Chapter 3

Experimental Details

3.1 Introduction

The experimental work consisted of two main phases: Direct pull-out test and post-mortem examination. In order to measure the intrinsic and apparent bond strength, the direct fiber pull-out test was used. By applying a pull-out load on a single FRP rod embedded in concrete, displacement (or slip) of the FRP rod relative to concrete at both the load and free ends was monitored. The first phase was focused on investigating the rod interface failure progression along the embedment length of the indented and sand coated FRP rod. The second phase was to determine the failure mode of the FRP reinforced concrete specimen by post-mortem examination of the tested samples.

3.2 Specimen

A schematic diagram of the specimen is shown in Figure 3.1. The specimen consisted of a cylindrical dimension of 12" x 6" (height x diameter). FRP reinforcement was embedded in the center of the concrete cylinder. The embeddment length of the FRP reinforcement was controlled by two PVC debonders. The PVC debonders at the load end of the FRP rod had a constant

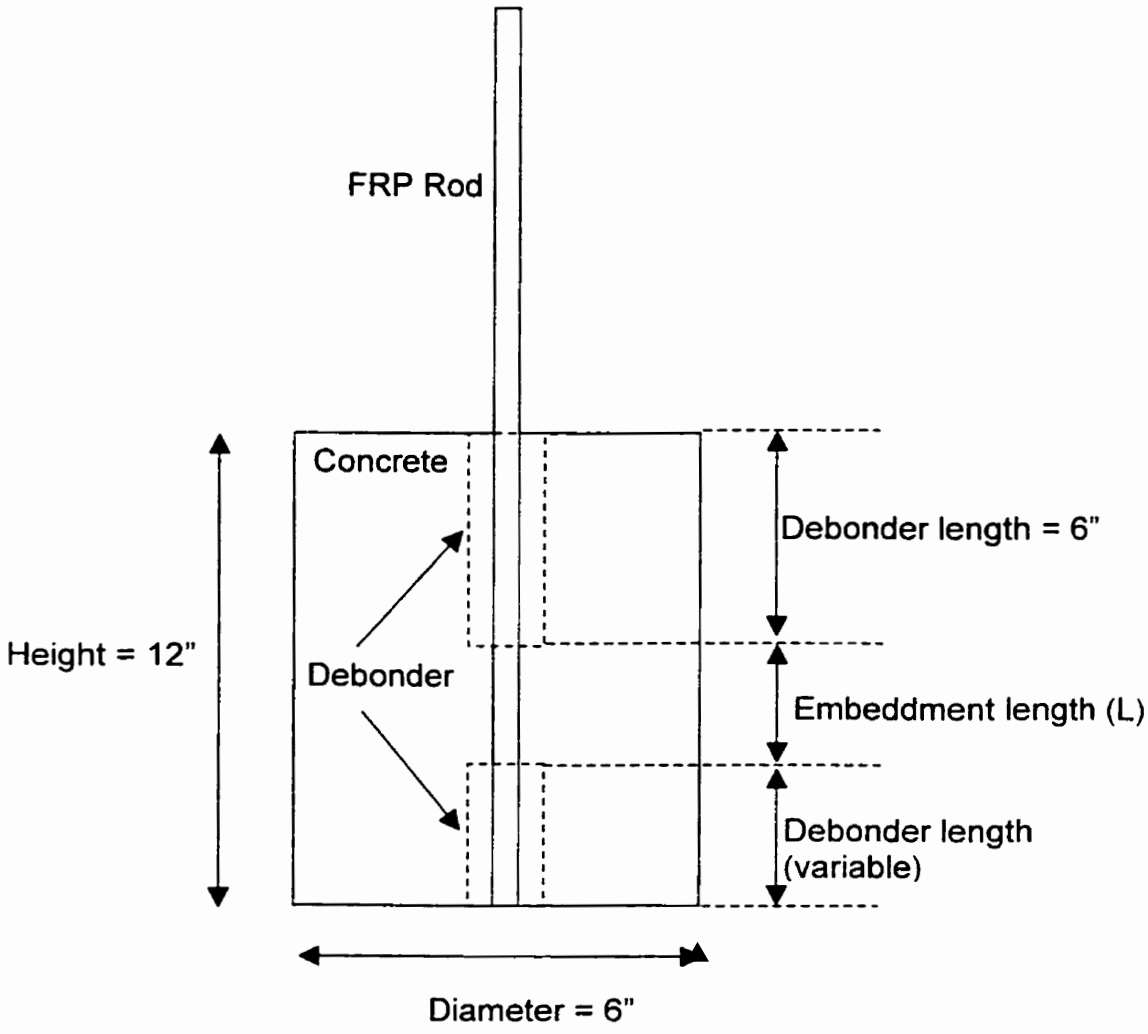

Figure 3.1 Schematic Diagram of Specimen

length of 6"; the length of PVC debonder at the free end was varied to obtain a specific embeddment length. The FRP rod was bonded to a metal tube (6" in length and 1.25" in diameter) using an epoxy. This aided in gripping of the FRP rod without damaging it during the pull-out test.

3.2.1 FRP Reinforcement

The FRP reinforcement rods used in the present experiment consisted of commercially available FRP rods such as C-BAR™ and ISOROD™. The mechanical properties of these FRP rods, which are provided by the manufacturer [14,15], are tabulated in Table 3.1. The selected FRP rods with several different surface geometries are illustrated in Figure 3.2.

A schematic of the C-BAR™ is shown in Figure 3.3. C-BAR™ is the trade name for the commercial available FRP rod, which is manufactured by Marshall Industries Composites Inc, USA. C-BAR™ is made of continuous glass fibers impregnated with an epoxy resin and manufactured by the pultrusion process. The surface of this type of FRP rod was indented to improve the mechanical interlocking with the concrete. The surface area (A) of the C-BAR™ used in determining interfacial bond strength is given in Equation 3.1.

Table 3.1 Mechanical Properties of GFRP Rods [14,15]

FRP Rod	Diameter mm	Specific Weight kg / m	Average Ultimate Tensile Strength MPa	Modulus of Elasticity GPa
C-BAR™	12.7	0.25	770	42
ISOROD™	12.7	0.25	683	40

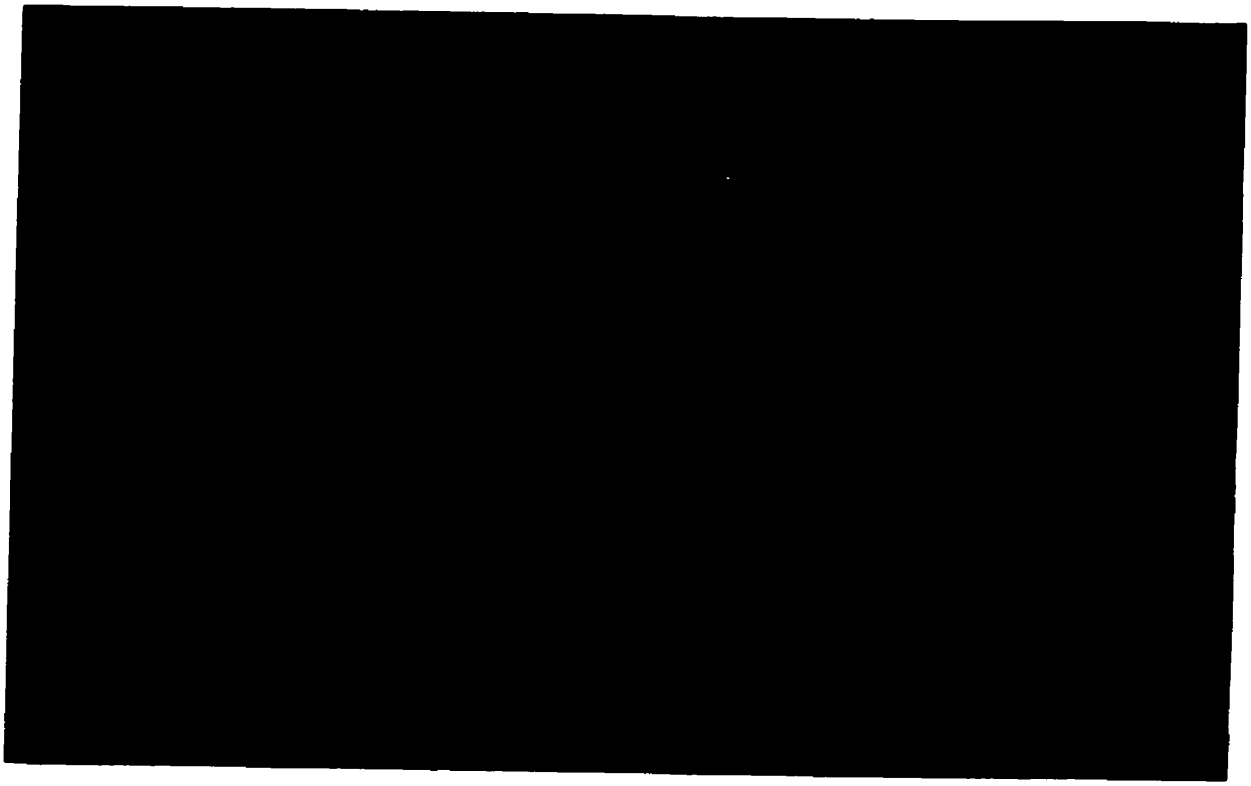

Figure 3.2 Tested FRP Rods

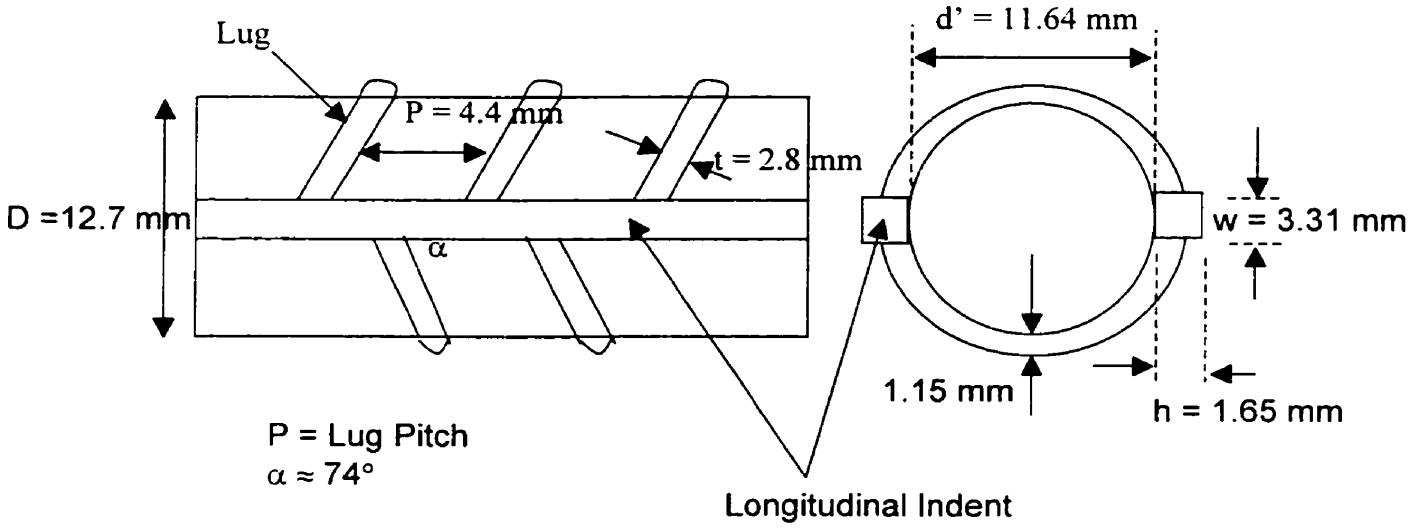

Figure 3.3 Surface Geometry of the C-BAR™

$$A = A_{rod} + N \times A_{lug} + A_{long} - A_{over} \qquad (3.1)$$

where A_{rod} = Total surface area without lug (D = 12.7 mm)

= D x L x π (D = Rod diameter, L = Embeddment length)

A_{lug} = Surafe area of one lug = $\frac{(d'+D)t\pi^2}{4\sin\alpha}$

N = Number of lug

A_{long} = Area of the longitudinal indent = $2\,(2h + w)\,L$

A_{over} = Overlap surface area = $\frac{4wL\sin\alpha + (d'+D)t\pi N}{2\sin\alpha}$

Classification labels and details on various C-BAR™ surface geometry that are used in this thesis are summarized in Table 3.2. Two different types of C-BAR™ were tested, as received C-BAR™ (RL series) and machined C-BAR™. As received C-BAR™ was used without additional surface-geometry modification and machined C-BAR™ was modified by removing the lug on the rod surface by machining in a lathe. This resulted in a C-BAR™ without any lug on the FRP rod is referred as machined C-BAR™ (M). Furthermore, by removing lugs alternately, C-BAR™ (SLC & TLC) with different pitch lengths were fabricated.

ISOROD™ is the trade name for the commercially available glass fiber reinforced plastic rod, which is manufactured by the Pultrall Inc, Canada. This type of GFRP rod is made of continuous longitudinal glass-fiber strands bound together with a thermosetting polyester resin and manufactured by the pultrusion process.

Table 3.2 Various Surface Geometries of C-BAR™

Label	**Lug Pitch (p) mm**	**Description**	**Note**
RL	4.40	Lug	As Received
SL	11.95	Lug	Machined
TL	26.90	Lug	Machined
M	--	Smooth	Machined

Two different surface geometries of ISOROD^{TM} were used for direct pull-out test, one with sand-coated particle on the rod surface and another one with smooth surface ISOROD without sand particle coating. Both types of ISOROD^{TM} are referred as SCC and SC respectively in this thesis. Measuring the actual surface area of the sand-coated ISOROD^{TM} was difficult. Therefore nominal diameter of the rod and embeddment length was used to calculate the surface area using equation 3.2.

$$A = D' \times L \times \pi \qquad (3.2)$$

Where A = Surface area

D' = Nominal diameter of the SCC rod (13.6 mm)

L = Embeddment length

3.2.2 Concrete

The concrete used in this study was a mixture of normal type-10 Portland cement, water, concrete sand and aggregate. The composition of the concrete mixture to yield the desired compressive strength, as suggested by Portland cement Association [16], is given in Table 3.3.

Table 3.3 Composition of Concrete Mixture [16]

Water **kg**	**Cement** **kg**	**Sand** **kg**	**Gravel (9.5 mm Max Size)** **kg**
15.875	34.020	68.494	95.256
Total volume of air entrained concrete prepared per batch = 94734.2 cm^3 Water / cement ratio = 0.5			

The concrete was cured for at least 28 days, in order to reach a desirable compressive strength. It was cured under room temperature and covered with an impermeable plastic sheet to maintain the moisture while curing. The compressive strength of the concrete was determined as per the ASTM standard (C39 - 86) [17], using cylindrical specimens (12" height x 6" diameter) fabricated from each batch of specimens. The average compressive strength of the concrete specimen is 49.77 ± 2.26 MPa (7.21± 0.33 ksi).

3.3 Direct Pull-out Test

The direct pull-out test was carried out by using a servo hydraulic loading machine (MTS) with a maximum loading capacity of 1000 kN. The MTS (Material Test System) was controlled by a control modular (810 MTS), which allowed either a constant loading rate or a constant displacement rate.

The detailed schematic of the pull-out test setup is shown in Figure 3.4. The FRP rod was gripped rigidly on the actuator side such that the top section of the concrete cylinder was pressed against a ½" thick steel plate. A thin layer of plaster was applied between the specimen surface in contact with the steel plate in order to ensure full-contact and proper alignment. During loading, the FRP rod was moving up. Hence the steel plate was bolted to the ground using two 2 ¼" diameter rods.

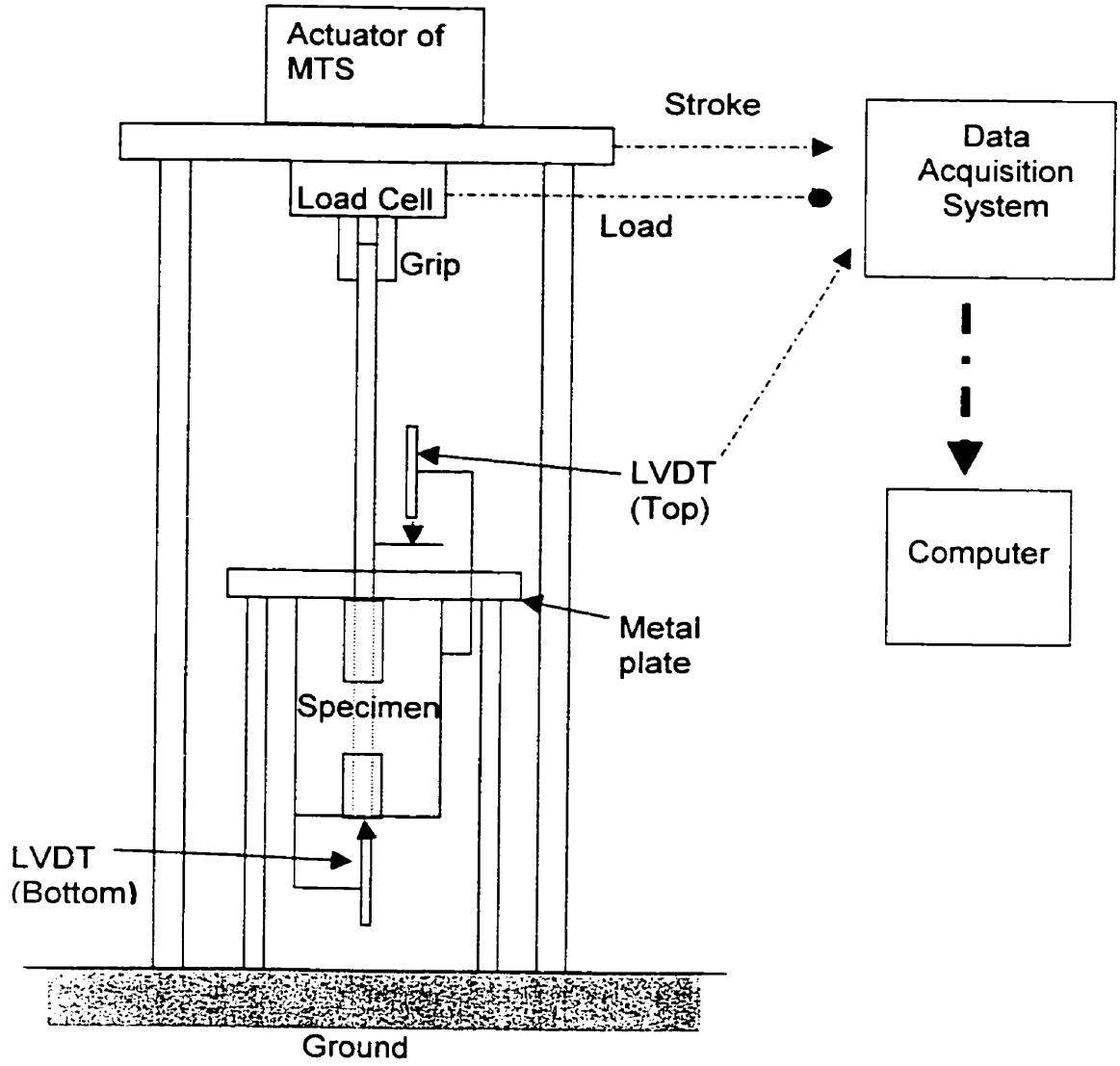

Figure 3.4 Direct Pull-out Test Setup

Displacement (slip) of the FRP rod with respect to the concrete, during the pull-out test was measured using a LVDT (Linear Variable Differential Transformer). Slip at both the load and free ends were measured using two LVDTs held rigidly by a custom designed fixture as shown in Figure 3.5. Load, actuator displacement and slippage of both the load and the free ends of the FRP rod were recorded using a computer and a data acquisition system.

3.4 Testing Procedure:

The direct pull-out test was divided into four parts. All the samples were tested at a selected displacement rate of 1.3 mm/min or otherwise stated. The first part was to determine the critical embedment length or development length for subsequent testing. Based on a simple shear lag theory, the critical length (L_c) may be predicted using Equation 3.3, if τ_b is known.

$$L_c = \sigma_u D / 4 \tau_b \qquad (3.3)$$

where σ_u = FRP rod ultimate tensile strength

D = FRP rod diameter

τ_b = FRP – concrete shear strength or interfacial bond strength

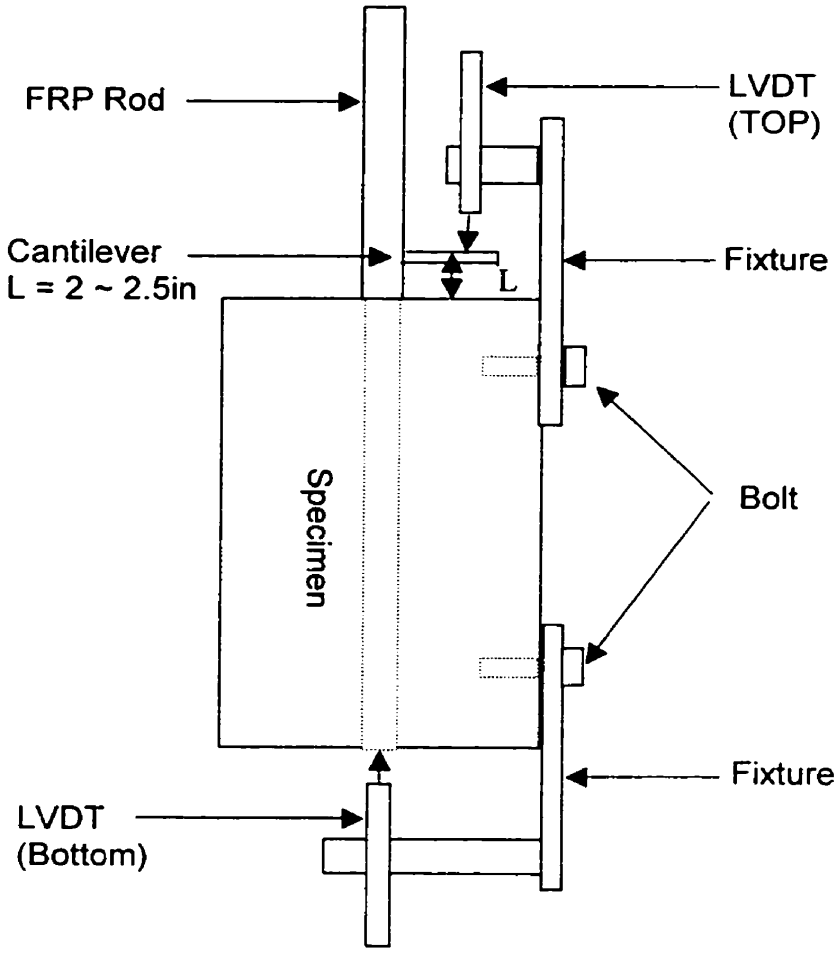

Figure 3.5 Locations of LVDTs

The critical embeddment length (L_c) is the embeddment length where fracture mode changes from interface failure to FRP failure. Alternatively, it can be determined experimentally as follows. Four different embedment lengths of the as-received C-BAR^{TM} (RL) and machined smooth C-BAR^{TM} (M), as tabulated in Table 3.4, were used. The tested samples were subjected to a post-mortem examination to confirm the failure mode.

After the critical embeddment length (L_c) of the as-received C-BAR^{TM} was known, an embeddment length, less than the critical length, was chosen for all the specimens in the subsequent testing. The suitability of this selected critical embeddment length to lead to interface failure was confirmed by testing the machined smooth C-BAR^{TM} (M series) with four different embeddment lengths.

The second part of pull-out test was focused on determining the intrinsic, apparent load and frictional resistance from the direct pull-out test. The fracture mode of the pull-out test specimens was examined by post mortem of selected specimens.

The third part of the pull-out test was to investigate the contribution of bearing resistance by studying the interfacial failure progression in specimens with lugs (RLC, SLC and TLC) and sand-particle coated specimen (SCC). The experiments were conducted by loading the specimen to a load level less than

Table 3.4 Summary of the Pull-out Test (Part 1)

Type of FRP Rod	Label	Surface Configuration	Rod Diameter mm	Pitch Length mm	Embedment Length mm	No of Specimens
As-received C-BAR	RLA	Lug	12.7	4.4	127.00	3
	RLB				95.25	3
	RLD				63.50	3
	RLE				31.75	3
Machined -BAR	MA	--	12.7	--	127.00	3
	MB				95.25	3
	MD				63.50	3
	ME				31.75	3

the maximum pull-out load (F_a). The maximum pull-out load of each type of specimens was determined in the second part of the pull-out test. Once the desired load was reached the specimens were unloaded. The tested samples were examined by post-mortem examination to determine the extent of the interfacial failure progression at the FRP-concrete interface. A summary of specimens used in part two and three of the experiment is given in Table 3.5.

The last part of the direct pull-out test was to investigate the effect of loading rate on apparent load for the RLD and SCC specimen. Two distinctly different displacement rates (0.26, 6.50 mm / min) were used to compare with a reference displacement rate (1.3 mm/min). A summary of this part of pull-out test is given in Table 3.6.

3.5 Post-mortem Examination

The goal of post mortem examination was to confirm the mode of failure and to measure the extent of lug failure in the interfacial region by dissecting the tested specimen.

One major requirement was to examine the interfacial region without disturbing the interfacial structure. Hence, the post-mortem process was conducted carefully to retain the original FRP-concrete interfacial structure. A 14" diamond blade cutter was used to dissect the 12" x 6" specimen to a distance of about 1"

from the FRP rod, as shown in Figure 3.6. The dissected sample was cleaned to remove any dirt from the surface of the sample. The sample was then opened with a chisel by applying a force on the on the dissected section as shown in Figure 3.6. The dissected samples were examined visually to determine the mode of fracture.

Table 3.5 Summary of the Pull-out Test (Part 2 and 3)

Types of FRP Rods	Label	Surface Geometry (Number of Lug) mm	Rod Diameter mm	Pitch Length mm	Embedment Length mm	No. of Specimen	% of Max. Load
C-BAR™	RLC	Lug (12)	12.7	4.40	88.9	3 1 1	100 85 60
	SLC	Lug (6)	12.7	11.95	88.9	3 1 1 3 1 1	100 80 70 60 40 30
	TLC	Lug (3)	12.7	26.90	88.9	3 1 1 1	100 75 50 35
	MC	Smooth (Machined)	12.0	--	88.9	3	100
ISORO D™	SSC	Sand Coated Surface	13.6	--	88.9	2 1 1 1	100 90 70 50
	SC	Smooth	12.5	--	88.9	2 1 1 1	100 90 70 50

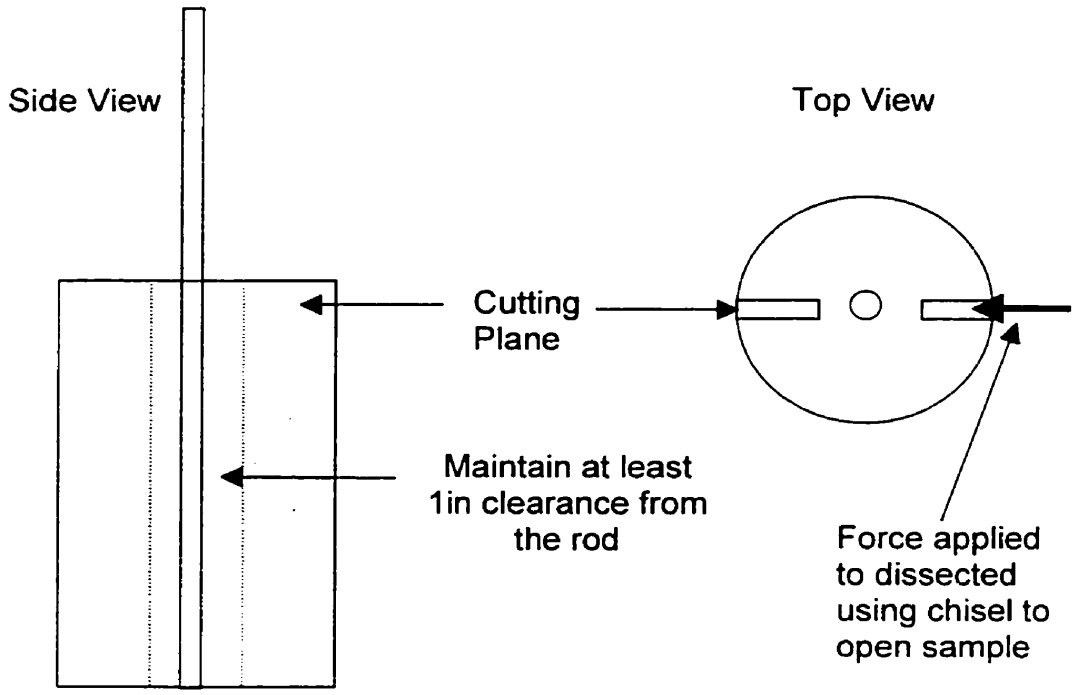

Figure 3.6 Post Mortem for Tested Sample

Chapter 4

Results and Discussion

4.1 Introduction

The results of direct pull-out test and post-mortem for various types of specimens are presented in this chapter. Two different types of commercially available FRP rod such as C-BAR™ and ISOROD™, were used for the present study. Additional surface modifications of the FRP rod were used to modify the pitch length between lugs. The experiment program was divided into four parts:

- Determine the critical embeddment length of as received (RL-series) and machined (M-series) C-BAR™
- Determine the intrinsic and apparent bond strength
- Study the interface fracture progression in both LC-series FRP rods (including RLC, SLC and TLC) and sand-particle coated FRP rod (SCC).
- Understand the effect of the loading rate on apparent interfacial bond strength for indented (RLD) and sand coated (SCC) FRP rod

The results for each part of these experiments are presented and discussed in this chapter.

4.2 Results

4.2.1 Determination of Critical Embeddment Length

Critical embeddment length (L_c) was determined to select an appropriate embeddment length that would yield interface failure for subsequent tests. A total of 12 samples were tested with 3 trials for each embeddment length. A summary of the pull-out test is shown in Figure 4.1a. Results for the individual test are tabulated in Table 4.1. Specimens RLA and RLB with embeddment length equal to 127.0 mm and 95.5 mm respectively failed by rod fracture while others exhibited FRP rod pull-out. This had been confirmed by post-mortem examination (refer to Figure A1 – A4 in Appendix). Though this critical length was theoretically calculated using a shear-lag model (Equation 3.3) to be 99.06 mm, the premature failure of FRP rod in these specimens is believed to be due to defective FRP rod. In order to ensure interface failure in the subsequent tests, an embeddment length equal to 88.9 mm (3.5") was selected. Results of the pull-out test for smooth machined C-BAR^{TM} (M-series), as shown Figure 4.1a, confirmed that the selected embeddment length was appropriate to yield interfacial failure. The apparent interfacial bond strengths for specimen that exhibited FRP rod pull-out are shown in Figure 4.1b.

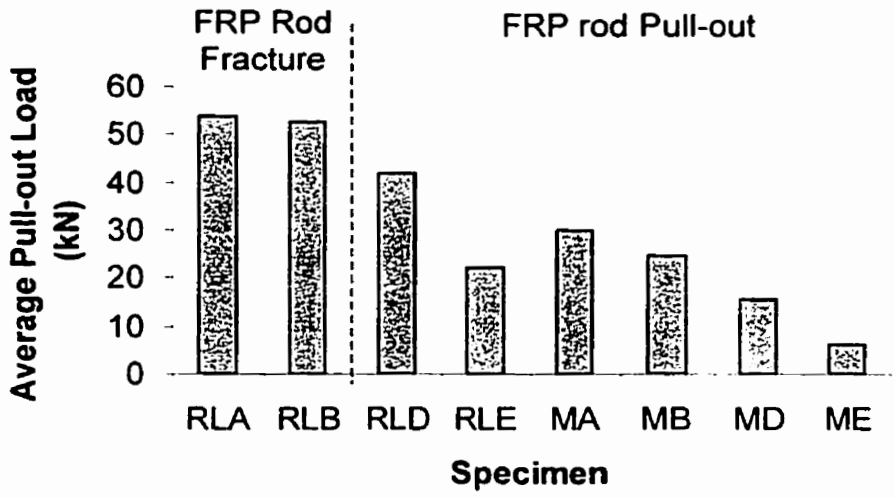

Figure 4.1a Summary of the Experimental Result in Part I

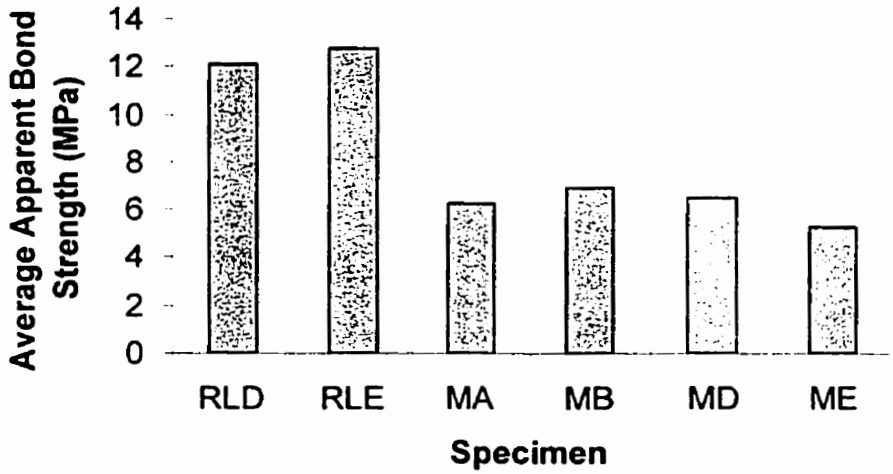

Figure 4.1b Average Apparent Bond Strength for Lugged and Machined FRP Rod

Table 4.1 Summary of the Pull-out Test in Part I

Specimen Type	Average Maximum Load kN	Average Apparent Shear Strength MPa	Average Tensile Strength MPa	Type of Fracture
RLA	53.69 ± 9.24	--	437.53 ± 75.30	F
RLB	52.59 ± 15.41	--	428.52 ± 125.54	F
RLD	42.09 ± 3.67	12.08 ± 1.05	--	I
RLE	22.19 ± 3.98	12.74 ± 2.29	--	I
MA	29.87 ± 4.02	6.25 ± 0.84	--	I
MB	24.84 ± 5.73	6.93 ± 1.60	--	I
MD	15.54 ± 6.70	6.50 ± 2.80	--	I
ME	6.30 ± 0.32	5.27 ± 0.27	--	I
F : Rod fracture; I : Interface failure				

4.2.2 Determination of the Intrinsic and Apparent Interfacial Bond Strength

To determine the intrinsic and apparent interfacial bond strength, direct pull-out tests were carried out on specimens made with FRP rods with different surface geometries such as lugged (RLC, SLC and TLC), sand coated (SCC), machined smooth (MC) and smooth FRP rod (SC). An embeddment length of 88.9 mm (3.5") was used for all tests.

The displacement (also referred as slip in this thesis) of the rod relative to concrete at load and free ends was monitored using two LVDTs located at both ends during the pull-out test. This relative displacement excludes the elastic elongation of the FRP rod. A sample plot of load verses slip is shown in Figure 4.2 for SC specimen. While the load-end of the FRP rod started to slip as soon as the experiment began, the free-end slip remained zero until an intrinsic load (F_i) is reached. Previous research (4, 8) has established that the shear stress, at any applied load, at the interface during direct fiber pull-out test is maximum at the load-end and decreases along the embeddment length of the FRP rod towards the free-end. Thus, the debonding progression begins at the load-end and propagates to the free-end of the FRP rod. Since, the free-end can only start to slip after the debonding has progressed completely throughout the entire embedment length. The load at which the free-end slip starts was taken to be the intrinsic load (F_i). Beyond F_i, the pull-out load continues to increase until the maximum pull-out load (F_a) and this is due to frictional resistance (F_f) between

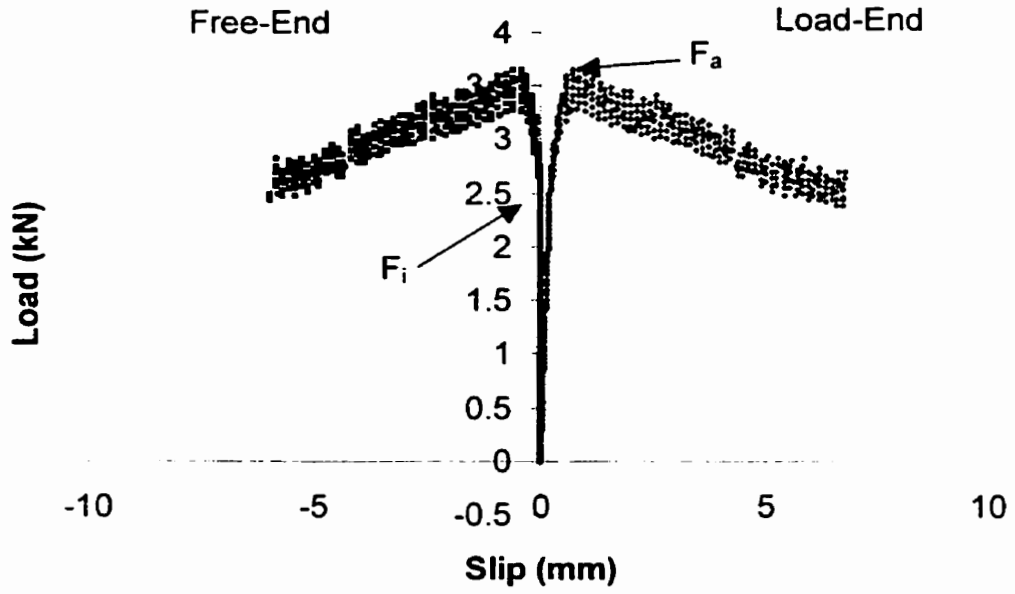

Figure 4.2 Load – Slip Plot for SC Specimen

the FRP rod and the concrete interface.

4.2.2.1 Intrinsic Bond Strength:

The intrinsic interfacial bond strength (τ_i) is determined using this intrinsic load (F_i) for specimens with various types of surface geometries and are shown in Figure 4.3 and are also tabulated in the Table 4.2. Ideally, the intrinsic bond strength should be independent of the surface geometries on the FRP rod and should be dependent only on the chemical bonding between the FRP rods and concrete and on the lateral pressure exerted on the FRP rod by the concrete. This lateral pressure is a function of dry shrinkage of the concrete and swelling of the FRP rod due to absorption of moisture by the rod matrix. Since the material and curing conditions remained the same, it would be expected that the intrinsic bond strength remain the same for all specimens. However a marginal increase in the value was observed in MC, SCC and LC samples as compared to SC sample. Possible reasons for this are:

1) Error in calculation of actual surface area, especially in SCC and MC samples where surface roughness was substantial. Area calculated using average FRP rod diameter did not take into account any increase in surface area due to surface roughness. Hence the bond strength calculated using average value are greater than bond strength based on actual surface area.

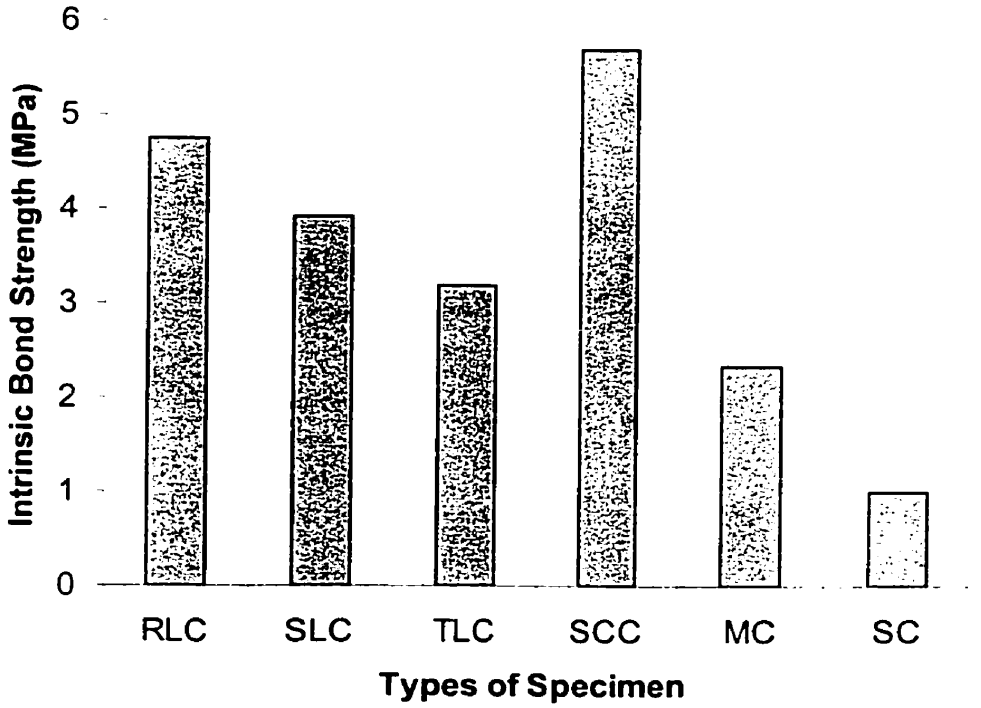

Figure 4.3 Summary of Average Intrinsic Bond Strength

Table 4.2 Summaries of the Average Intrinsic Load and Interfacial Bond Strength

Specimen Type	Average Intrinsic	
	Load kN	Bond Strength MPa
RLC	23.46 ± 3.36	4.75 ± 0.22
SLC	17.61 ± 4.85	3.92 ± 1.08
TLC	13.59 ± 1.08	3.19 ± 0.25
SCC	21.58 ± 0.02	5.68 ± 0.01
MC	9.48 ± 0.70	2.34 ± 0.17
SC	3.59 ± 0.84	1.01 ± 0.24

2) The measured intrinsic bond strength corresponds to completion of debonding rather than start of debonding.

Testing, using dye penetrant to accurately measure the load corresponding to the start of debonding proved to be difficult. Hence, the load corresponding to completion of debonding was taken to be the intrinsic load. During progression of debonding, the frictional and bearing resistance could have contributed to the overall increase in load and hence the measured intrinsic bond strength. A post-mortem examination of specimens loaded to F_i indicates that the surface of the FRP rod was not damaged at F_i. This suggests that F_i is due to chemical bonding and lateral pressure.

4.2.2.2 Apparent Interfacial Bond Strength:

The results of the average apparent load and interfacial bond strength are tabulated in Table 4.3 and are plotted in Figure 4.4. For LC specimens with lugs, the apparent bond strength increases in the order of TLC, SLC and RLC. In other words, the apparent bond strength of the indented FRP rod (LC-series) increased with the number of lugs in the FRP rod, since increasing the number of lugs increases the bearing resistance of the reinforcement. In the specimens where friction resistance is dominant the surface roughness increased in the order of SC, MC and SCC. Hence their apparent shear strengths also increased in that

Table 4.3 Summaries of Average Apparent Load and Interfacial Bond Strength

Specimen Type	Average Apparent	
	Load **kN**	**Bond Strength** **MPa**
RLC	57.13 ± 0.24	11.57 ± 0.05
SLC	39.46 ± 3.69	8.79 ± 0.82
TLC	33.79 ± 5.30	7.92 ± 1.25
SCC	51.42 ± 15.00	13.53 ± 3.94
MC	23.56 ± 3.21	5.82 ± 0.79
SC	4.26 ± 0.04	1.2 ± 0.21

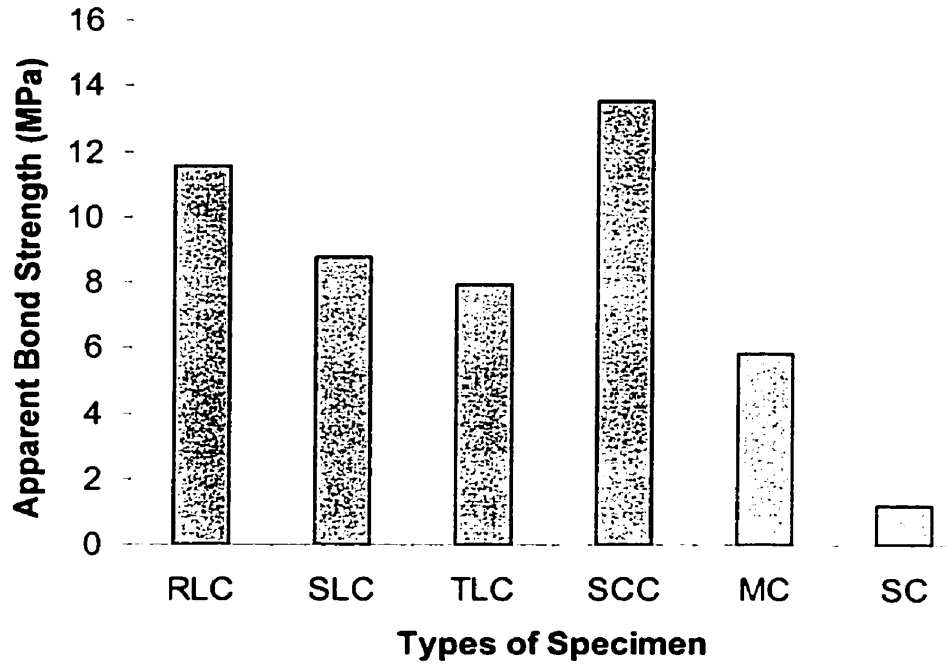

Fig 4.4 Summary of Average Apparent Bond Strength

order, as shown in Figure 4.4. Typical load-slip plots for SC, MC, SCC and TLC specimens are given in Figures 4.2 and 4.5 - 4.7 respectively. It can be observed that the load increased beyond F_i until F_a, when the load dropped to F_f for all specimens. This increase in load from F_i to F_a is due to contributions from both frictional and bearing resistance.

Role of Friction:

Beyond F_i the FRP rod will move relatively against concrete and friction will play a crucial role in determining the load required for displacing the FRP rod relative to concrete. A post mortem of the TLC samples loaded to F_a indicated that all the lugs have been sheared off. Similarly the post-mortem of SCC samples exhibits a complete shearing off sand particles from the FRP rod. Since these lugs and sand particle are the sources of bearing resistance, it can be concluded that the bearing resistance is not presented beyond F_a. If there were no frictional resistance, then the load would continue to drop to zero. However, the load drops to a value of F_f before increasing in LC, SCC, MC samples and remaining almost constant for the SC samples until the entire rod is pulled out. Hence the minimum load F_f has to be due to contribution from frictional resistance. The F_f was taken to be the frictional load and used in determining frictional stress values tabulated in Table 4.4 and plotted in Figure 4.8a and 4.8b for various specimens.

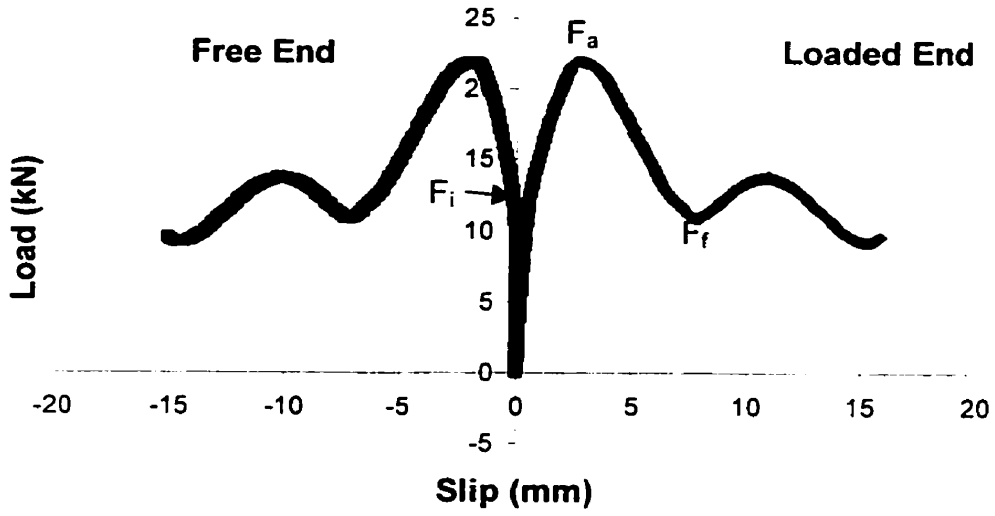

Figure 4.5 Load – Slip Plot for MC Specimen

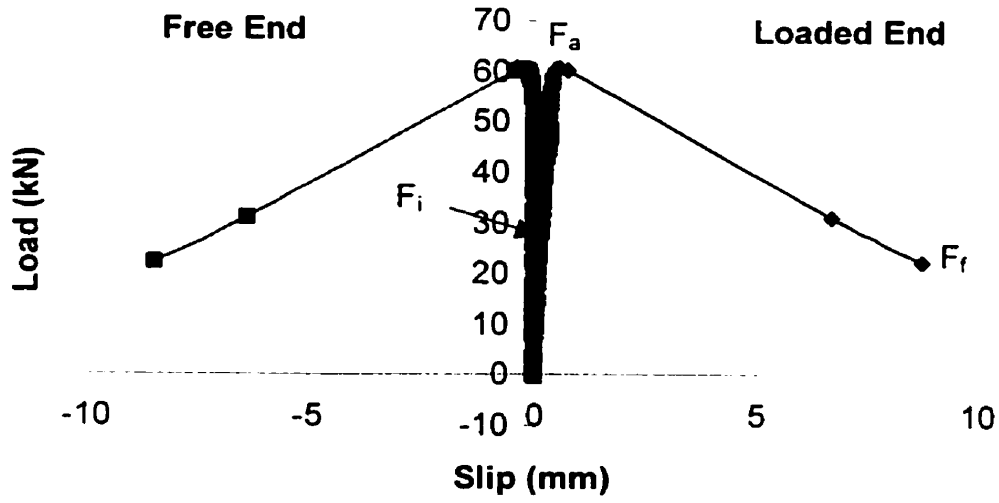

Figure 4.6 Load – Slip Plot for SCC Specimen

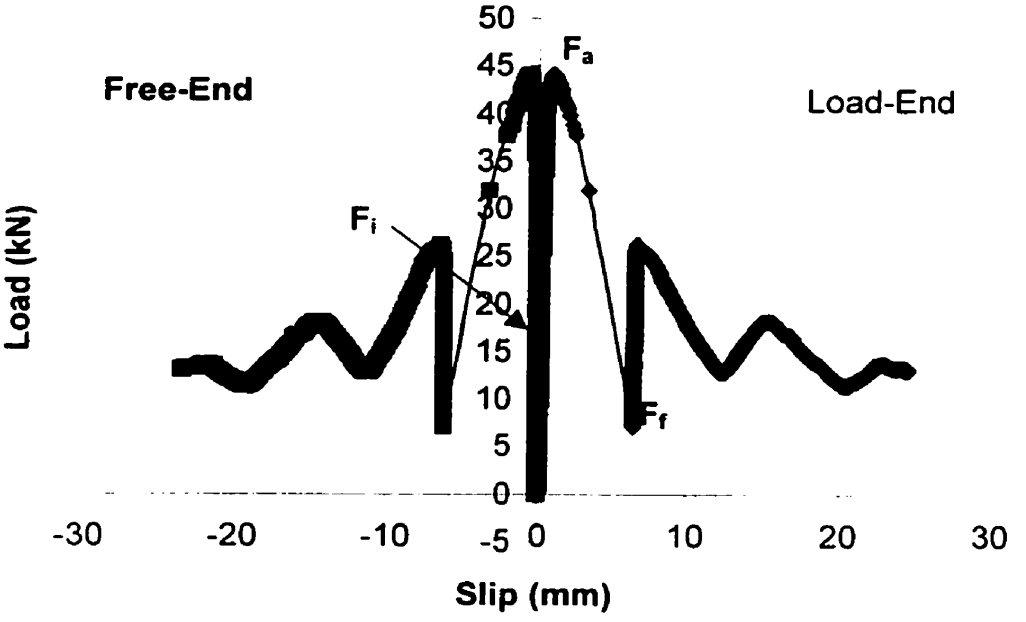

Figure 4.7 Load – Slip Plot for SLC Specimen

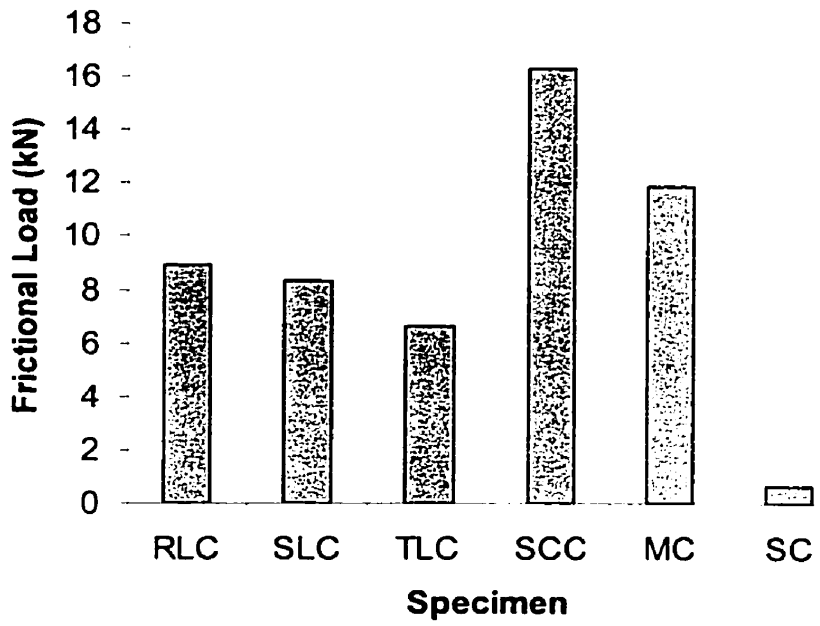

Figure 4.8a Summary of Frictional Load

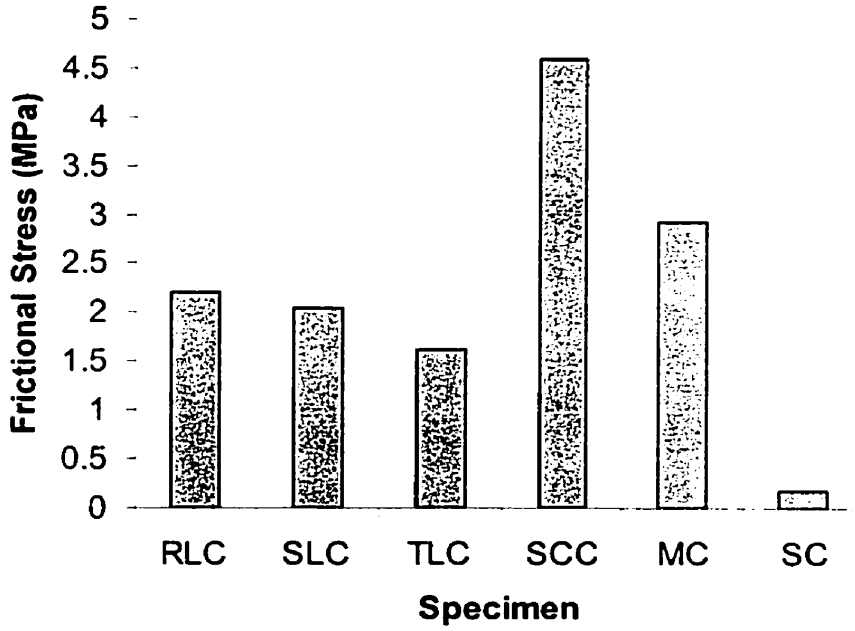

Figure 4.8b Summary of Frictional Stress

Table 4.4 Summary of Nominal Frictional Load and Stress

Specimen	Nominal Frictional Load kN	Nominal Frictional Stress MPa
RLC	8.94 ± 2.06	2.21 ± 0.51
SLC	8.30 ± 1.06	2.05 ± 0.26
TLC	6.61 ± 0.31	1.63 ± 0.08
SCC	16.32 ± 4.75	4.60 ± 1.34
MC	11.86 ± 0.85	2.93 ± 0.21
SC	0.67 ± 0.32	0.19 ± 0.09

In the smooth rod (SC) specimens, bearing resistance does not exist due to lack of surface geometry that can provide mechanical interlocking to the concrete. The frictional resistance is expected to be minimal. In the ideal case, frictional resistance should be close to zero for the smooth rod and the apparent and intrinsic load should be the same. However, there is a marginal contribution from frictional resistance as indicated by the difference between intrinsic load (F_i) and apparent load (F_a) in Figure 4.2. Post-mortem examination of the pulled-out sample indicated that the surface of the SC rod and concrete was clean with very little scoring as shown in Figure 4.9a and 4.9b. This is in accordance with minimal measured frictional stress and indicates that the bonding is mainly due to the lateral pressure and chemical bonding. The oscillations, which are found in the curve, are thought to be due to the surface roughness of the SC rod.

When compared to the SC specimen, the machined smooth FRP rod (MC) exhibits a higher apparent load due to relatively higher surface roughness of the rod. It results in a higher frictional load and stress as shown in Figures 4.8a and 4.8b respectively. Similar to SC specimen, this post-mortem examination revealed clear FRP rod and concrete surface as shown in Figure 4.10. However, the level of scratches on the surface was relatively higher in accordance with higher frictional stress.

In the SCC specimen, frictional resistance is further enhanced by the sand-particles bonded to the FRP rod surface. Hence, the magnitude of frictional

Figure 4.9a Post-mortem Examination on SC specimen (SC rod) (F_a = 100%)

Figure 4.9b Post-mortem Examination on SC specimen (Concrete Interface)

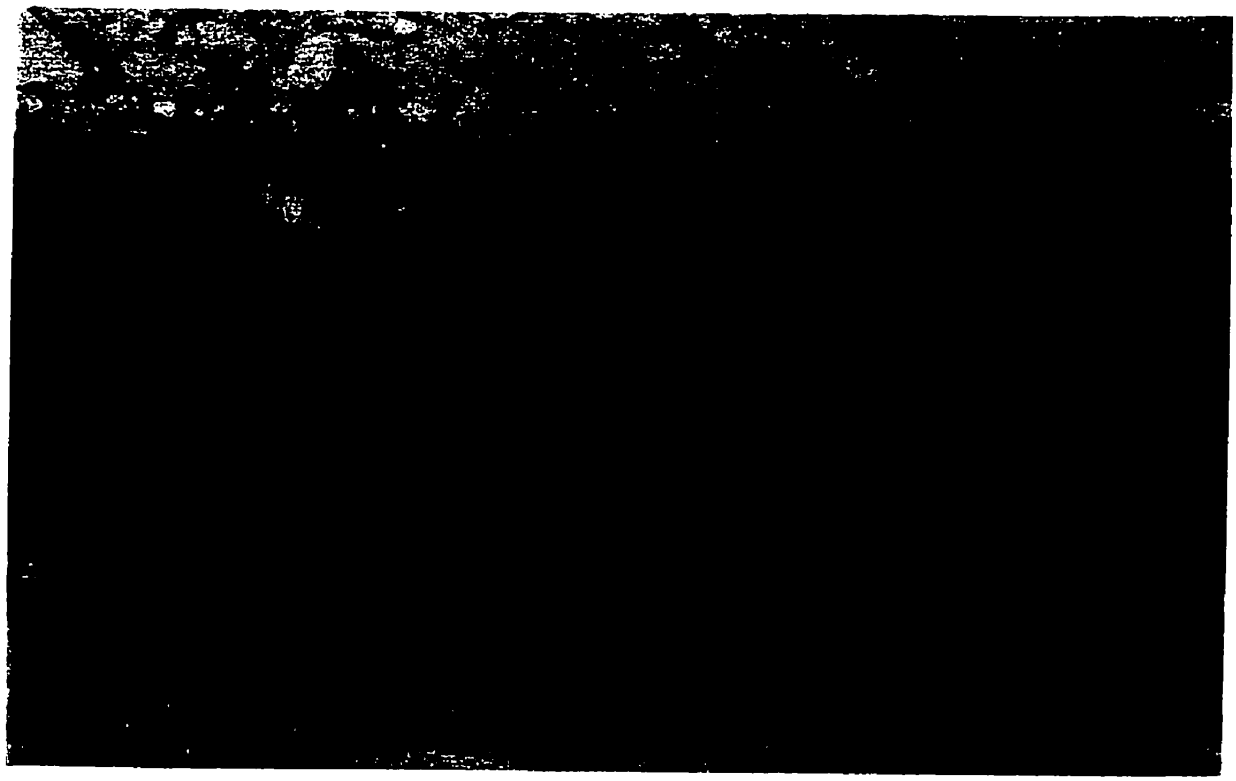

Figure 4.10 Post-mortem Examination on MC specimen (F_a = 100%)

stress is more than that of SC and MC specimens. Post-mortem examination of the tested SCC specimens showed that the sand particle sheared off completely at F_a as shown in Figure 4.11. Hence the measured frictional stress may not correspond to actual friction that contributed to the load increase between F_i and F_a. Post-mortem of samples that loaded to levels between F_i and F_a indicates that frictional resistance changed continually between F_i and F_a.

Post-mortem examination of fracture surface of SCC specimen loaded to F_a revealed completion of shearing off sand particles from FRP surface and this suggested that the friction changed continually between F_a and F_i in the SCC specimens (Figure 4.11). This is corroborated by progressive debonding of the sand particles on the fracture surface of SCC specimens that is loaded to a load levels in between F_i and F_a. As shown in Figure 4.12, the embeddment length to which sand particles sheared is plotted as a function of load (refer to Figure B1 – B4 in appendix for additional figures from post-mortem examination). Obviously, the length, which sand-particles are debonded, increases with increase in applied load. Hence, this might have caused a changing in frictional resistance between F_i and F_a. This would mean that the rate of loading will alter the F_a and hence comparison of apparent shear strength values should be made only at comparable test speeds. This would explain the difference in maximum pull-out loads obtained by Al-Zahrani [8] and Benmokrane et al. [7], as shown in Table 1.4. Further investigation is needed to measure accurately the change in this stress during testing.

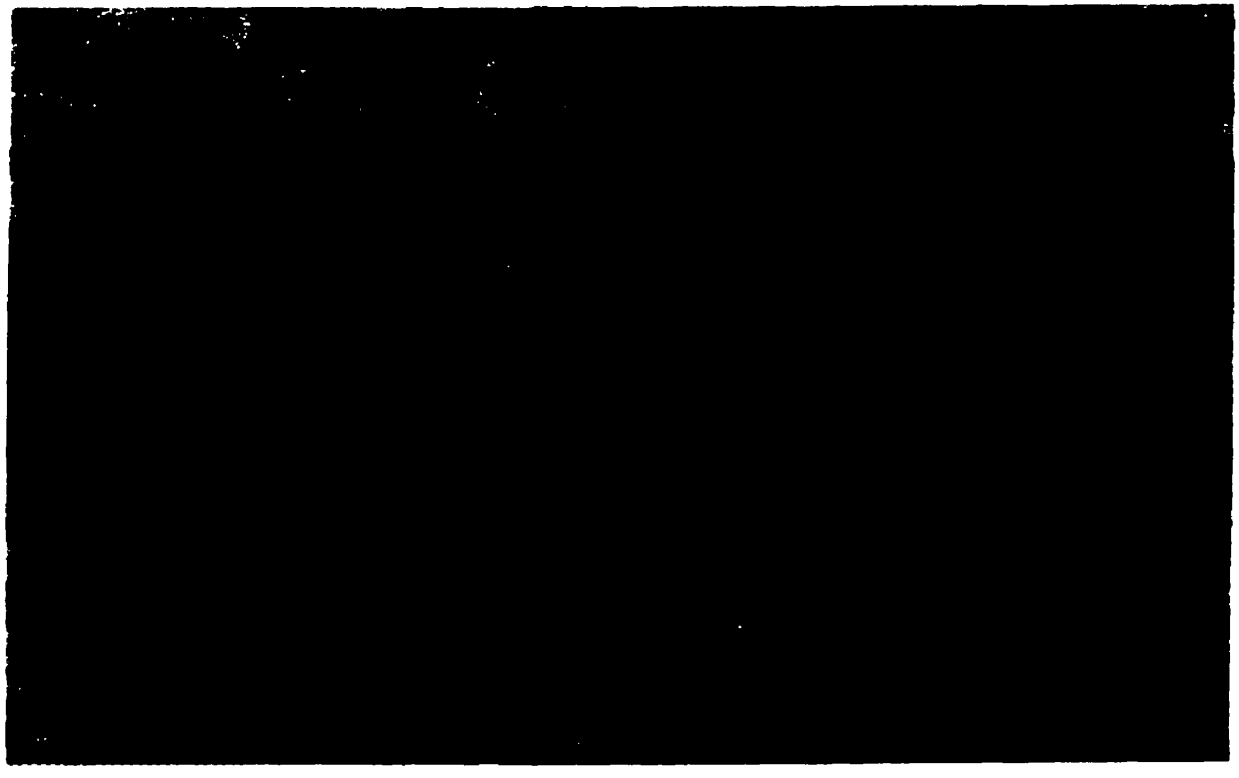

Figure 4.11 Post-mortem Examination on SCC specimen (F_a = 100%)

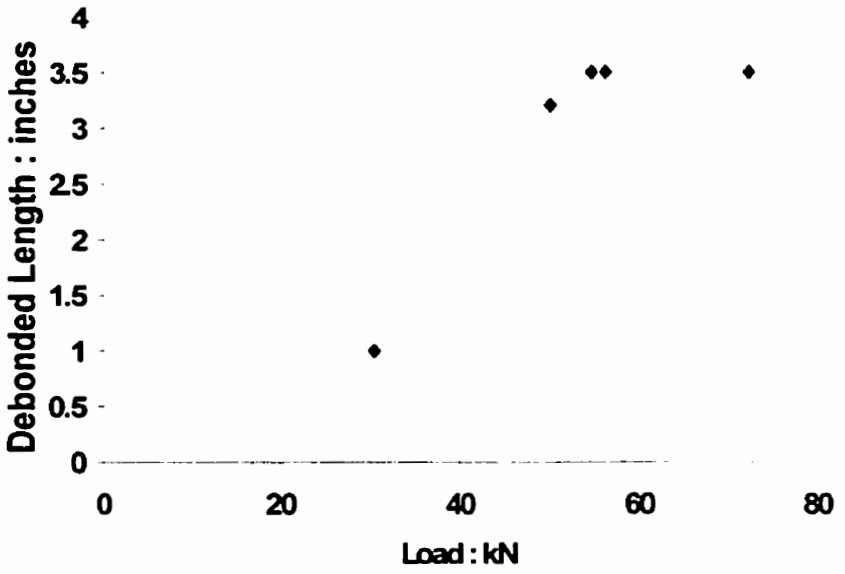

Figure 4.12 Debonded Length (sand-particle) vs. load

Finally for the LC specimen (including specimens RLC, SLC and TLC), the frictional shear stress (τ_f) was higher than the SC specimens, comparable to MC, and less than the SCC specimen. The higher frictional resistance finds in specimen with lug (LC-series) as compares to SC specimens is believed to be due to the additional frictional resistance is caused by sheared off lugs that is caught in between the concrete and FRP rod. Since the number of lugs increase from TLC, SLC to RLC samples, the marginal increase in frictional stress from TLC to RLC is believed to be due to an increase in the number of sheared off lugs of the FRP rod caught between the FRP and concrete.

Role of Bearing Resistance

As discussed in Chapter 2, the load F_a has been taken to be: $F_a = F_i + F_f + F_b$ (equation 2.3). Thus, the bearing resistance (F_b) contribution was determined by subtracting the measured value of F_a, F_i and F_f. The values are tabulated in Table 4.5 and plotted in Figure 4.13. It can be observed that bearing resistance is almost negligible in the case of SC and MC samples. This is expected since the amplitude of the roughness is very small. However, substantial bearing resistance was recorded for both the SCC and LC-series specimens (including RLC, SLC and TLC). It can be observed that the average bearing stress for the TLC and SLC specimens comparable to that of the SCC specimen. The maximum value of F_b for RLC sample indicates that the bearing resistance, which is offered by the lug, is higher.

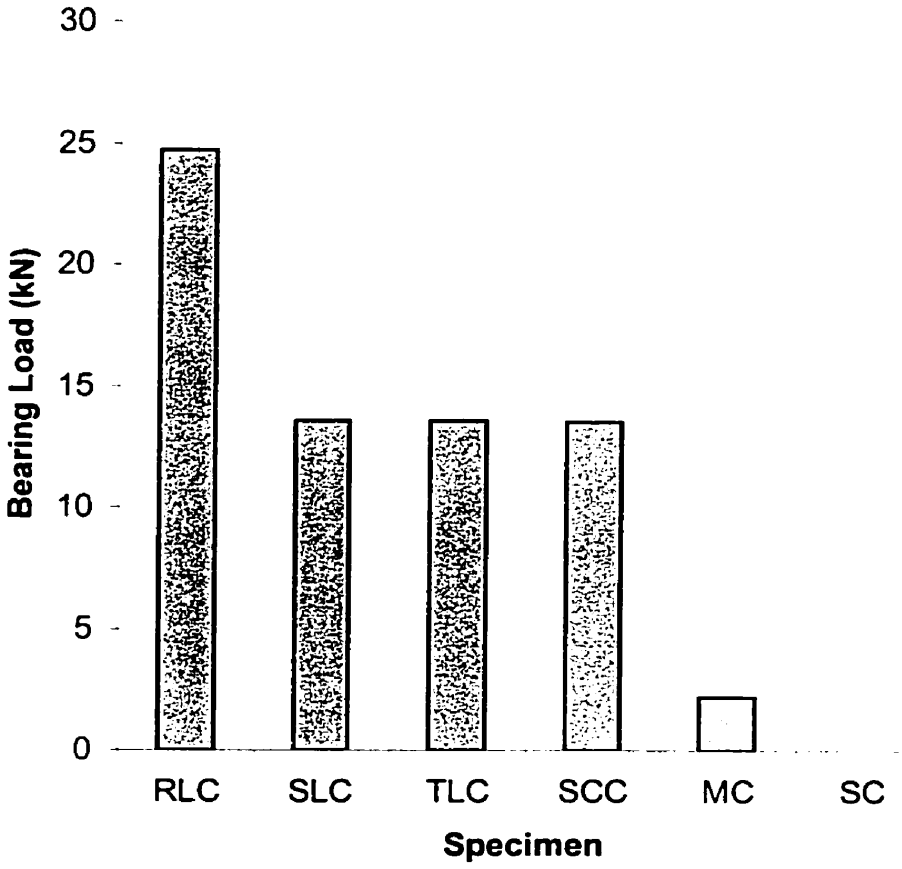

Figure 4.13 Average Bearing Resistance

Table 4.5 Average Bearing Resistances

Specimen	**Average Bearing Resistance (F_b) KN**
RLC	24.72
SLC	13.55
TLC	13.59
SCC	13.52
MC	2.21
SC	0.00

than that of sand particle. As expected the bearing resistance increased with number of lugs from specimen TLC to RLC. Fracture mode of specimens subsequent to debonding was by shearing of lugs. Post-mortem examination of specimens, which were loaded to load < F_a, indicated that shearing of a number of lugs is a function of load. In order to characterize the lug failure progression and to relate it to the applied load, LC specimens were loaded to various load level (between F_i and F_a) and unloaded. The fracture surface of these samples was examined through post-mortem and the number of sheared-off lugs was determined. As shown in Figure 4.14, in specimen was loaded to 70% of its maximum pull-out load, three lugs were fractured near the load-end. For specimen that was loaded to F_a, all the lugs were sheared as shown in Figure 4.15 (refer to Figures C1 – E3 in appendix for additional figures from post-mortem examination). Load versus number of sheared lugs is plotted in Figure 4.16 and the results are tabulated in Table 4.6. The linear relation confirms that the majority of load increases between F_a and F_i is due to bearing resistance of the lugs. The extrapolated value of F_a for a value of 0 sheared lugs is observed to be more than the intrinsic load. The difference between F_a and F_i (at x=0), which is due to frictional contribution, is about 12 $\pm$ 4 kN. The measured frictional stress as tabulated in Table 4.4 is of similar value and this validates the research approach followed in this thesis. The average shearing load per lug is shown as 2.6 kN (slope of the best-fit line in Figure 4.16). Using this value the average shear stress of one lug is calculated to be 17.08 MPa. This is similar to that

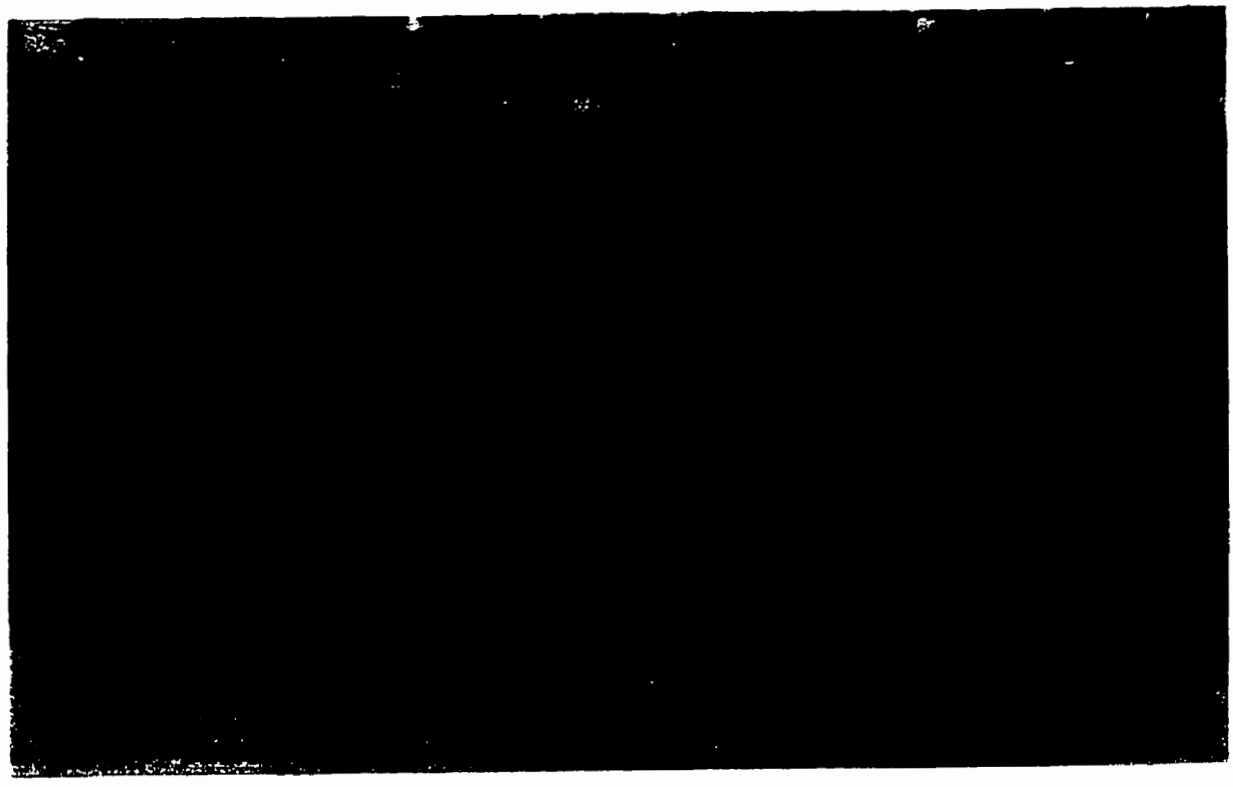

Figure 4.14 Post-mortem Examination on RLC specimen (F_a = 70%)

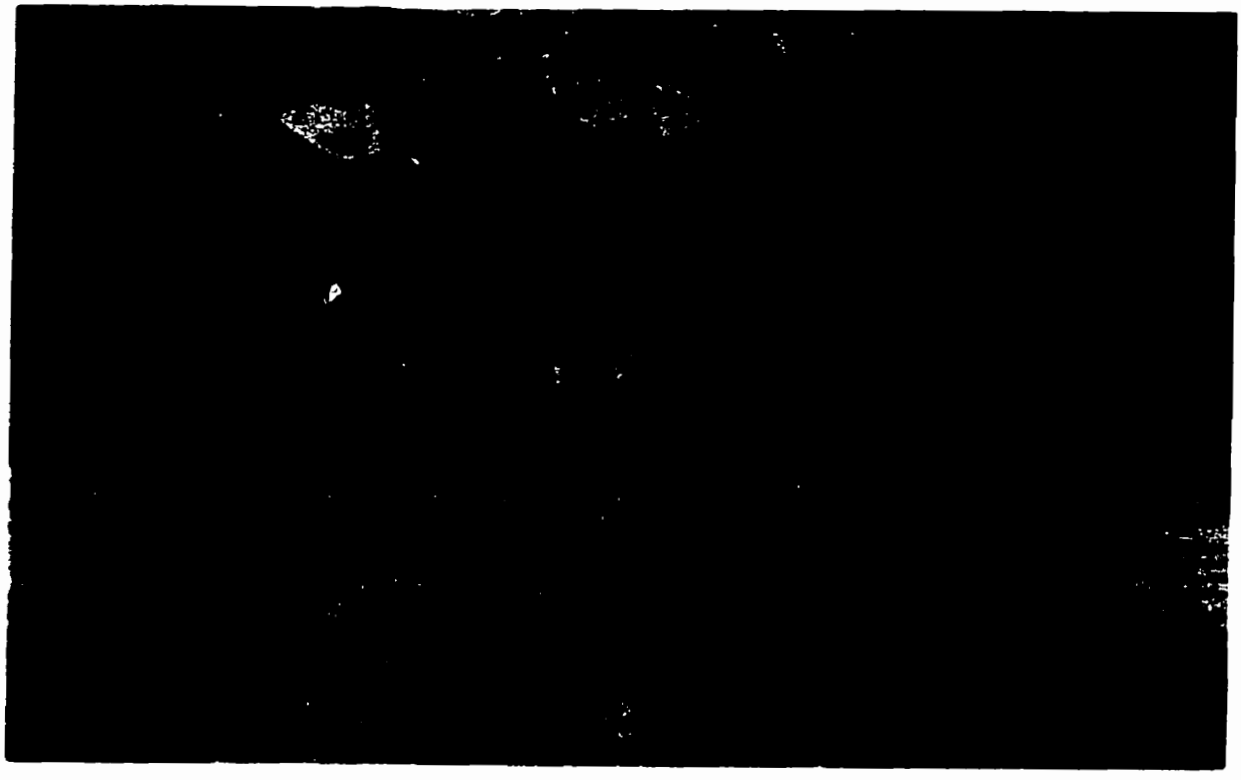

Figure 4.15 Post-mortem Examination on RLD specimen (F_a = 100%)

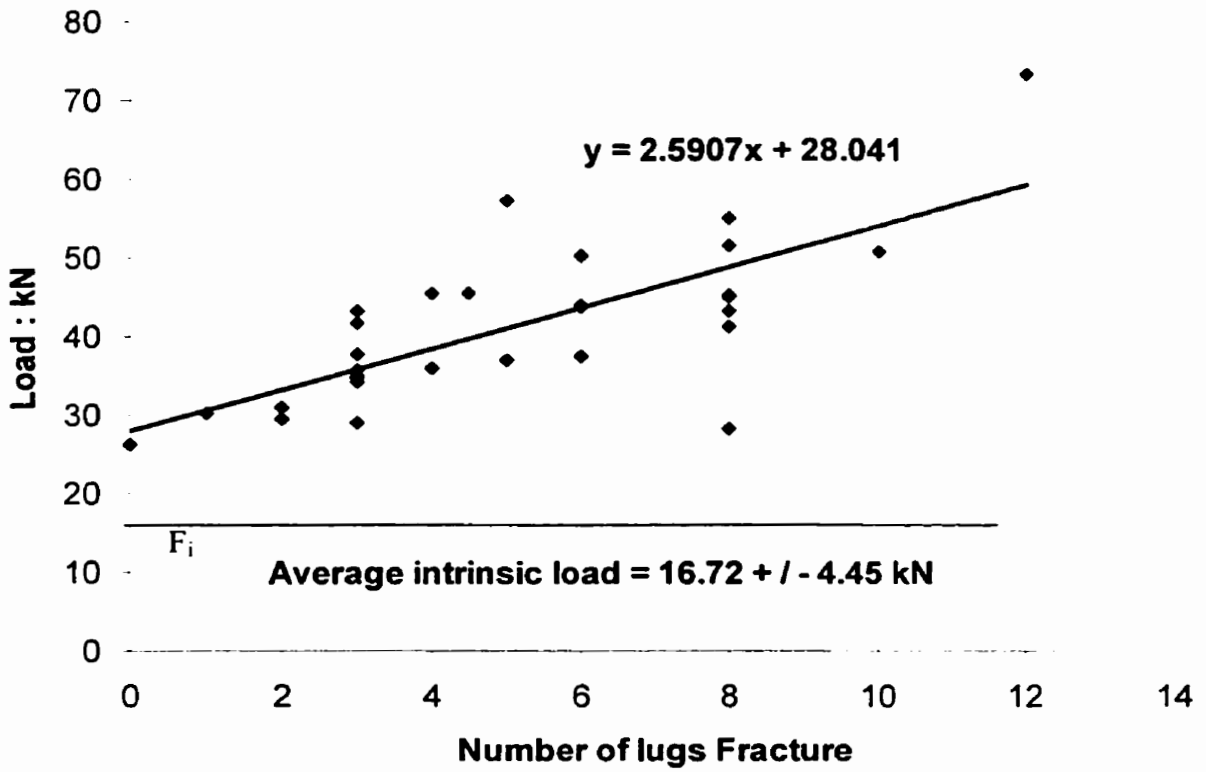

Figure 4.16 Load vs. Number of Lug Fracture for Intended Specimen

Table 4.6 Summary of Number of Lug Fracture verses the Pull-out Load

Sample	Load kN	Percentages of Maximum Load %	Number of Lugs Fractured / Total Lugs
RLB	73.28	100	12/12
	45.60	60	4.5/12
	50.67	70	10/12
RLD	51.61	100	8/8
	26.28	50	0/8
	35.9	70	4/8
	45.47	90	4/8
RLE	28.12	100	4/4
	26.23	100	4/4
RLC	57.31	100	12/12
SLC	34.18	60	3/6
	37.52	100	6/6
	43.73	100	6/6
	43.96	100	6/6
	50.29	100	6/6
	41.72	80	3/6
	30.90	60	2/6
	34.93	60	3/6
	15.00	30	0/6
	20.65	40	0/6
	30.30	60	1/6
	36.99	70	5/6
RLD	41.28	100	8/8
	45.11	100	8/8
	55.10	100	8/8
	43.28	100	8/8
	45.20	100	8/8
	28.22	100	8/8
TLC	34.77	100	3/3
	28.89	100	3/3
	35.79	100	3/3
	43.30	100	3/3
	37.69	100	3/3
	25.22	75	2/3
	16.93	50	0/3
	12.80	35	0/3

obtained by Al-Zahrani [8]. Hence, once the shear strength (τ_s) of the lugs is obtained, the bearing resistance contribution to the F_a can be determined using equation 4.1.

$$F_b = \tau_s A_l N \quad (4.1)$$

Where A_l = Area of lug

N = Number of lugs

However such a determination is not straight forward for SCC and MC specimen since the bearing resistance is caused by mechanical interlocking of the concrete with the cavities (due to roughness) on the FRP rod surface. A very accurate characterization of roughness and surface area due to this roughness is required for prediction using equation 4.1.

The load-slip behavior for the LC specimens between F_i and F_a will vary depending on the lug failure. As shown in Figure 4.17, the slopes are identical before F_i for all three load-slip plots. However, the slopes differ between F_i and F_a. The slope of the curves decreases with the increase in the pitch of the lugs. This indicates that the progressions of failure are different for these specimens. Beyond F_a, the rate of drop in load increases with the decrease in pitch length i.e. is in the order of TLC, SLC and RLC. Since a sharp drop in load corresponds to a sudden fracture of unsheared lugs at F_a, it can be concluded that the shearing

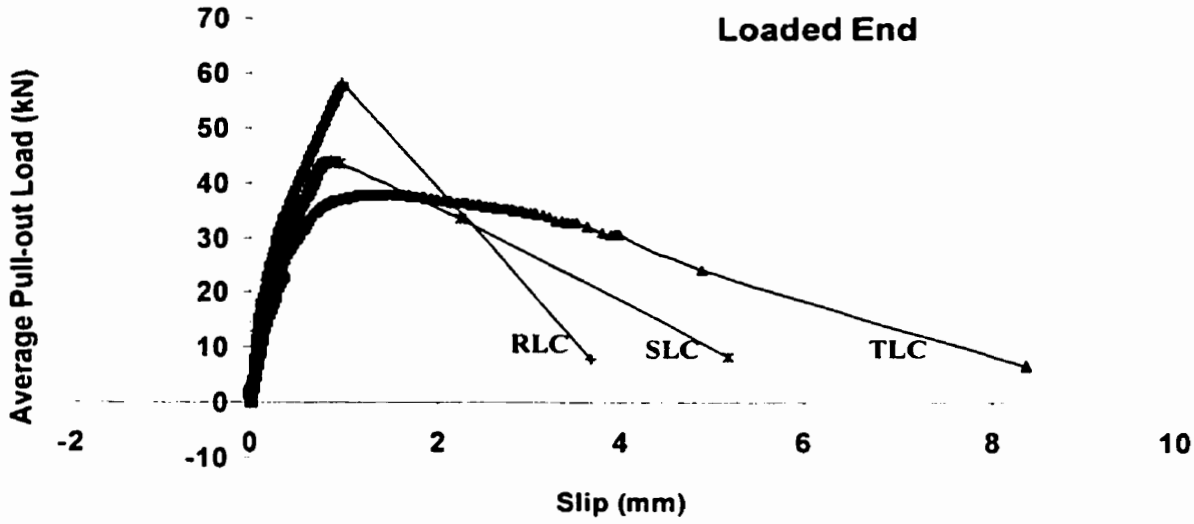

Figure 4.17 Load – Slip Plots for Indented Specimens

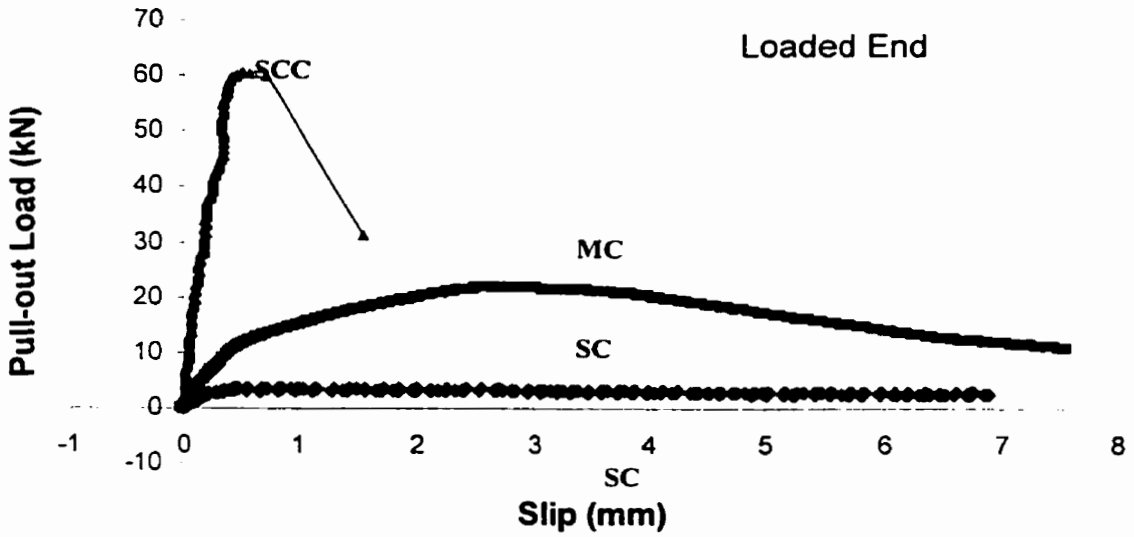

Figure 4.18 Load – Slip Plots for SCC, MC and SC Specimen

of lugs were completed before reaching F_a for the TLC samples. However, for the SLC and RLC samples, not all the lugs were sheared off before reaching F_a and were resulting in a rapid drop in load. Similarly, for the SCC specimen the rapid drop in load as shown in Figure 4.18 corresponds to sudden shearing of the sand particles on the rod. For the MC and SC specimens, such a sudden load drop was not observed due to lack of bearing resistance.

4.2.3 Effect of Loading Rate on Apparent Bond Strength

Results discussed in the previous section have shown that the frictional resistance contributes significantly to the measured apparent bond strength. Hence, the effect of loading rate on apparent bond strength would be significant. Experiments were carried out on SCC and RLD specimens at different loading rates to determine the effect of loading rate. Three distinctly different displacement rates (6.5, 1.3 and 0.26 mm / min) were used. The result of this experiment are plotted in Figure 4.19a and 4.19b and tabulated in Table 4.7. As shown in Figure 4.19a, the average apparent load for SCC specimens increases with increase in displacement rate indicating that frictional resistance and loading rate play a major role in the measured apparent bond strength for SCC specimen. However, for the RLD specimens as shown in Figure 4.19b, the effect of displacement rate on apparent load is not significant. This confirms the results shown in Figure 4.8 and 4.9 that this specimen has relatively less contribution from frictional resistance than bearing resistance.

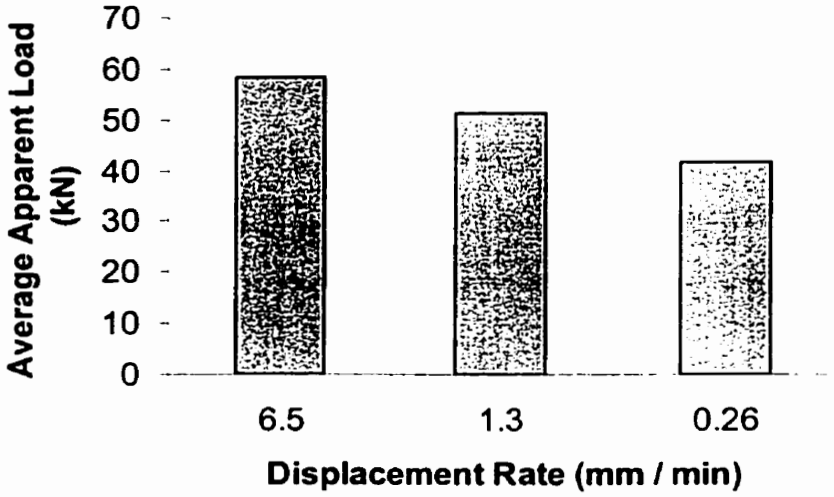

Figure 4.19a Loading Rate vs. Apparent Load Sand Coated Specimen (SCC)

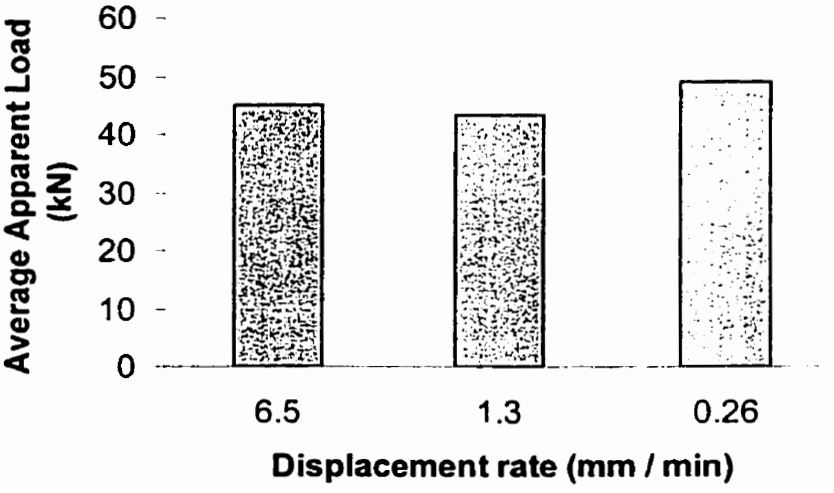

Figure 4.19b Loading Rate vs. Apparent Load Specimen with Lugs (RLD)

Table 4.7 Results of Displacement Rate and Average Apparent Load

Specimen	Displacement Rate (mm/min)	Average Apparent Load (kN)
SCC	6.5	58.42 ± 3.08
	1.3	51.42 ± 15.08
	0.26	41.90 ± 2.42
RLD	6.5	45.11 ± 0.00
	1.3	43.24 ± 2.77
	0.26	49.19 ± 8.36

4.3 Summary

In summary, experimental results have conclusively shown that the apparent load and hence apparent interfacial bond strength is due to contribution of mechanisms such as chemical bonding, confinement pressure, frictional resistance and bearing resistance. Depending on the surface geometry of the FRP rod, the contribution from each of these mechanisms varies. A summary of the contributions of each mechanism to the apparent bond strength of each specimen is plotted in Figure 4.20 and tabulated in Table 4.8.

For the SC specimen, the smooth surface provides relatively less frictional resistance and no bearing resistance. Hence the majority of contribution comes from chemical bonding and confinement pressure. However, for the MC specimen, the roughness amplitude of the smooth machined surface of the FRP rod provides additional frictional resistance, which is equivalent to 50% of the apparent load. Therefore, the effect of bearing resistance on apparent bond strength of this specimen is negligible. For the SCC specimen, the contribution of frictional resistance to apparent load is higher than bearing resistance. This is also the reason for higher sensitivity of apparent load of the SCC specimen to the loading rate. The apparent interfacial bond strength increases with loading rate. However, for the LC specimens, the apparent load is dominated by bearing resistance, due to the mechanical interlocking provided by the lugs. The contribution of the bearing resistance is about twice the frictional resistance,

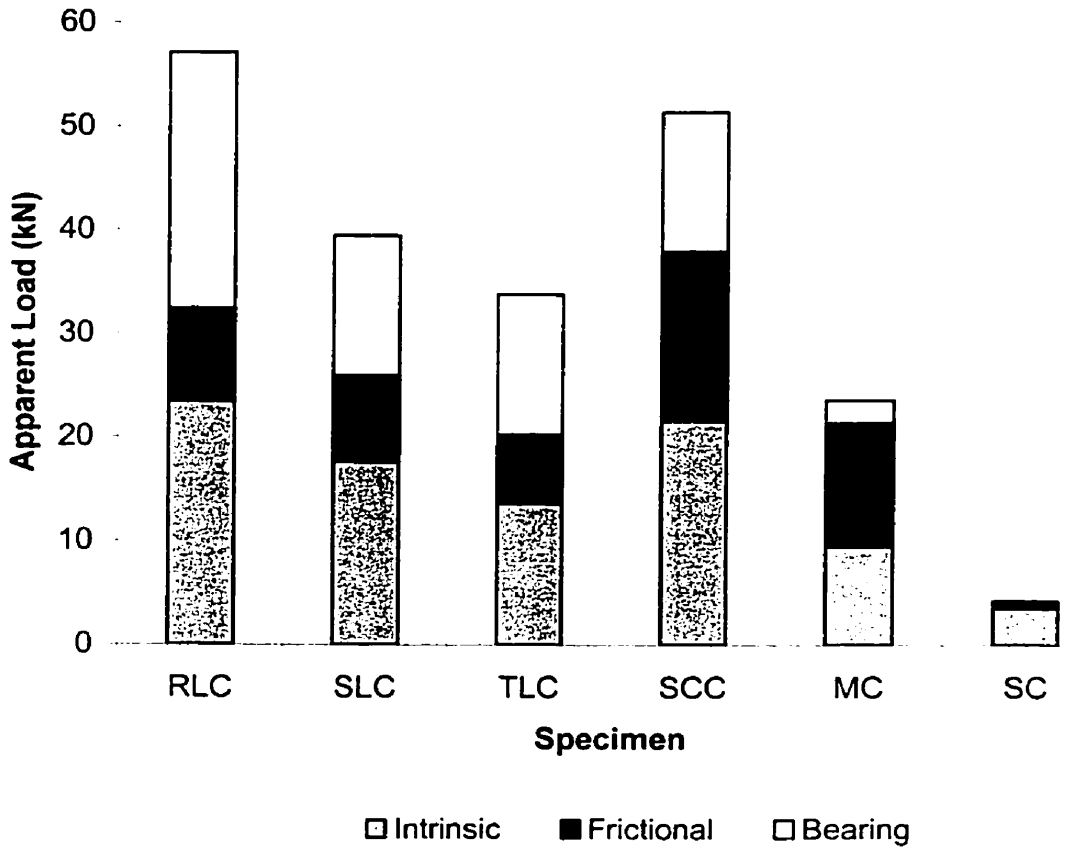

Figure 4.20 Summary of Contribution of Bonding Mechanism to Apparent Load

Table 4.8 Summary of Contribution of Bonding Mechanism to Apparent Load

Specimen	Average Intrinsic Load KN %	Average Frictional Resistance KN %	Average Bearing Resistance KN %	Average Apparent Load KN
RLC	23.46 41.06	8.94 15.65	24.72 43.27	57.13
SLC	17.61 44.25	8.30 20.86	13.55 34.05	39.46
TLC	13.59 40.22	6.61 19.56	13.59 40.22	33.79
SCC	21.58 41.97	16.32 31.74	13.52 26.29	51.42
MC	9.48 40.24	11.86 50.34	2.21 9.38	23.56
SC	3.59 84.27	0.67 15.73	0.00 0.00	4.26

hence the loading rate does not have the same effect on LC specimen as it does on the SCC specimens.

The apparent load and apparent bond strength can be predicted using equation 2.3. F_i can be predicted using interfacial bond strength and area of the contact surface on the present study, variation in the F_i and τ_i was observed from specimen to specimen. Since F_i corresponded to the completion debonding, careful experimentation is required to measure actual intrinsic bond strength.

F_f can be predicted using equation 4.2

$$F_f = \mu N \qquad (4.2)$$

Where μ = Frictional coefficient

N = Force normal to the interface

This force normal to the interface (N) is due to lateral pressure exerted by concrete on FRP. Further experimentation is required to obtain these values.

Finally, bearing resistance (F_b) can be predicted by using equation 4.1. Validation of this equation for LC specimens has been discussed in the previous section. However, as mentioned in the previous sections, validation of this equation for SCC, MC and SC specimens requires further experimentation.

Chapter 5

Conclusions and Recommendations

5.1 Conclusion

The results obtained in this study show that the bond strength between FRP – concrete is due to mechanisms such as chemical bonding, confinement lateral pressure, frictional resistance and bearing resistance. Bond strength, which is corresponding to chemical bonding and confinement pressure exerted on the FRP by dry-shrinkage and FRP swelling, is defined as intrinsic interfacial bond strength. Apparent interfacial bond strength is defined as maximum pull-out load, which is a summation of intrinsic load, frictional and bearing resistance, divided by the total contact area. Both the intrinsic and apparent bond strength is measured using direct pull-out test for FRP rods of varying surface roughness and geometries. Depending on the surface roughness and geometry, contributions from each of these bonding mechanisms vary.

A summary of the experimental results is presented below:

- SC specimens with a smooth surface recorded the lowest apparent interfacial bond strength (i.e. pull-out strength). Due to lack of surface roughness, the contribution to this strength was mainly due to chemical

bonding and confinement pressure. Contribution from bearing resistance was negligible and frictional resistance was marginal.

- With MC, and SCC specimens, the contribution due to both frictional and bearing resistance increased. However the contribution from the bearing resistance was found to be less than that from the frictional resistance. Since SCC specimens had a higher surface roughness amplitude than the MC specimens, the apparent interfacial bond strength was higher for SCC specimens than the MC specimens.

- With LC specimens, the bearing resistance from lugs was the major contributor resistance to the apparent interfacial bond strength. With increase in number of lugs from TLC to RLC, the bearing resistance contribution also increased.

- Loading rate influenced the apparent interfacial bond strength of the sand particle coated FRP rod (ISOROD^{TM}), due to relatively higher contribution (about 30%) from the frictional resistance to apparent bond strength. However, for the FRP rod with lugs (C-BAR^{TM}), the influence of the loading rate is lower due to relatively lower contribution of frictional resistance to the apparent bond strength.

Based on these results, it can be concluded that:

- Contribution from intrinsic bonding mechanisms such as chemical bonding and confinements pressure alone is not sufficient to achieve high FRP-concrete bond strength.

- Further improvement of the apparent bond strength can be achieved by additional mechanisms such frictional resistance and bearing resistance is definitely required.

- Bearing resistance appears to contribute more than frictional resistance for the specimens with lug. However, frictional resistance appears to contribute more than bearing resistance for sand particle coated specimens.

- Careful design of roughness amplitude and lug dimensions is required to achieve optimum interfacial bond strength.

5.2 Recommendations

Ascertaining the critical length (L_c) for commercially available FRP is critical to construction application (L_c) can be determined using equation 3.3. In the case of conventional design, critical length ($L_{c,a}$) is based on apparent bond strength (τ_a) as given in equation 5.1.

$$L_{c,a} = \sigma_u D / 4 \tau_a \qquad (5.1)$$

The precise understanding of debonding progression in the FRP – concrete interface is required since the experimental results of this study indicate that the debonding of FRP – concrete interface begins before F_i is reached. Moreover, beyond F_i, fracture progression initiates at the surface geometry of the FRP rod. Thus, a design of the critical length ($L_{c,i}$), which is based on intrinsic interfacial bond strength (τ_i) as given in equation 5.2, is conservative as no knowledge in fracture progression is required.

$$L_{c,i} = \sigma_u D / 4 \tau_i \qquad (5.2)$$

In this study, intrinsic bond strength (τ_i) is measured as the completion instead of the initiation of debonding between FRP and concrete interface. The initiation of the debonding corresponding to pull-out load still has not been studied. Hence, further investigation on the initiation of the debonding is required.

To have a better understanding of the intrinsic and apparent bond strength, following are some recommendations for the future works:

- To study the effect of dry-shrinkage of concrete during hydration process to the intrinsic bond strength.

- To study the effect of swelling of FRP due to moisture absorption to the intrinsic bond strength.

- To study the effect of surface geometry on strain distribution along the embeddment length.

References

1. Nanni, C. E.bakis, T. E. Boothby. "Test Methods for FRP-Concrete Systems Subjected to Mechanical Loads: State of the Art Review." Journal of Reinforced Plastics and Composites 14, (June 1995), pp. 524 – 558.

2. J. Freimanis, C.E Bakis, A. Nanni and D. Gremel. (1998). "A Comparison of Pull-out and tensile Behaviors of FRP Reinforcement for Concrete." Second International Conference on Composite in Infrastructure. H. Saadatmanesh and M. R. Ehsani, Ed. Tucson, AZ, (1998), pp 52 – 65.

3. B. Tighioart, B. Benmokrane, D. Gao. (1998). "Investigation on the Bond of Fiber Reinforced polymer (FRP) Rebars in Concrete" Second International Conference on Composite in Infrastructure. H. Saadatmanesh and M. R. Ehsani, Ed. Tucson, AZ, (1998), pp 102 – 112.

4. Benmokranne, B. Tighiouart, O.Chaallal. "Bond Strength and Load Distribution of Composite Reinforcing Bars in Concrete." ACI Materials Journal. May – June (1996). pp. 246 – 253.

5. M. M. Al-Zahrani, U. Al-Dulaijan, A. Nanni, C. E. Bakis, T. E. Boothby. "Evaluation of Bond Using FRP Rods With Axisymmetric Deformations" Technical Report.

6. E. Bakis, V. S. Uppuluri, A. Nanni, T. E. Boothby. "Analysis of Bonding Mechanisms of Smooth and Lugged FRP Rods Embedded in Concrete." Composites Science and Technology 58 (1998), pp. 1307 – 1379.

7. Benmokrane, D. MacEachern, M. T. T. That, B. Zhang. "Evaluation of Bond Characteristics of GFRP Rebars Embedded in Polymer and Normal Cement Concretes." Technical Report No. 7, University of Sherbrooke, 1999.

8. M. M. Al-Zahrani. "Bond behavior of Fiber Reinforced Plastic Reinforcements with Concrete." PhD Thesis. The Pennsylvania State University. (Dec 1995)

9. H. C. Boyle, V. M. Karbhari. "Investigation of Bond Behavior Between Glass Friber composite Reinforcements and Concrete" 1994, Polym – Plst. Technol. Eng., 33(6), pp. 733 - 753

10. J. S. Huang, M. T. Chen. "Effect of Interfacial Thickness and Stiffness on the Stress Distributions in Fibre Reinforced Cementatious Composites." Journal of Material Science 32 (1997), pp. 5143 – 5154.

11. H. Abrishami, D, Mitchell. "Analysis of Bond Stress Distributions in Pullout Specimens." Journal of Structural Engineering, (March 1996), pp. 255 - 261

12. Y. W. Chen, V. C. Li. "Effects of Transition Zone Densification on Fiber / Cement paste Bond Strength Improvement." Advance Cement based materials 5, (Jan 1997), pp. 8 – 17.

13. Bentur, S. Diamond, S. Mindess. "The Microstructure of the Steel Fibre-Cement Interface." Journal of materials Science 20, (1985), pp. 3610 – 3620.

14. Marshall Industries Composites Inc. "C-BAR Reinforcing Rods" (1995)

15. Pultrall Inc. " ISOROD – Glass Fiber Composite Rebar for Concrete Technical Data." (Feb 1992).

16. Portland Cement Association. "Design and Control of concrete Mixture." 7th Edition

17. ASTM. "Standard Test Method for Compressive Strength of Cylindrical Concrete Specimens." C 39 – 86.

Bibliography

1. S. Diamond, D. Bonen. " A Re-Evaluation of Hardened Cement Paste Microstructure Based on Backscatter SEM Investigations." Materials Research Society Symposium Proceedings Microstructure of Cement-Based System 370, Boston, (1995), pp. 13 – 22.

2. C. M. Neubauer, T. B. Bergstrom, K. Sujata, Y. Xi, E. Jagarboczi, H. M. Jennings. "Drying Shrinkage of Cement Paste as Measured in an Environmental Scanning Electron Microscope and Comparison with Microstructural Models." Journal of Material Science 32 (1997), pp. 6415 – 6427.

3. W. D. Bascom, K-J. Yon, R. M. Jensen, L. Cordner. "The Adhesion of carbon Fibers to Thermoset and Thermoplaastic Polymers." J. Adhesion, 1991, Vol. 34, pp. 79 – 98.

4. W-M Lin, T. D. Lin, C. L. Hwang, Y. N. Peng, "Fundermental Study on Hydration of Cement and Cement Minerals with Steam." ACI Materials Journal, Vol. 95, pp. 37- 49.

5. D. R. Mumm, K. T. Faber. "Effect of Reinforcement Surface Morphology on Toughening of Brittle – Matrix Components." ACI SP-156, pp. 181 – 191

6. D. R. Mumm, K. T. Faber. "Interface Design in Brittle – Brittle Systems." ACI SP-156, pp. 131 – 141

7. E. Cosenza, G. Manfredi, R. Realfonzo. "Behavior and Modeling of Bond of FRP Rebars to Concrete." Journal of Composites for construction (May 1997), pp. 40 – 51.

Appendix

Table A Results From Direct Pull-out Test on RL-series Specimen (Test 1)

Trial	Specimen	Maximum Pull-out Load (F_a) kN	Apparent Interfacial Bond Strength (τ_a) MPa	Ultimate Tensile Strength (τ_u) MPa	Type of Fracture
1	RLA	53.52		438.69	F
2		63.02		516.56	F
3		44.54		365.08	F
	Average	53.69 ± 9.24		440.11 ± 75.30	
1	RLB	36.02		295.25	F
2		51.20		419.67	F
3		49.85		408.61	F
	Average	52.59 ± 15.41		428.52 ± 125.54	
1	RLD	46.59	13.37		I
2		38.95	11.03		I
3		38.95	11.18		I
	Average	41.32 ± 4.67	11.86 ± 1.31		
1	RLE	21.55	12.37		I
2		26.46	15.19		I
3		18.57	10.66		I
	Average	22.19 ± 3.98	12.74 ± 2.29		
F: Rod Fracture; I : Interface Failure					

Table B Results From Direct Pull-out Test on M-series Specimen (Test 1)

Trial	Specimen	Maximum Pull-out Load (F_a) kN	Apparent Interfacial Bond Strength (τ_a) MPa	Type of Fracture
1	MA	34.23	7.16	I
2		26.30	5.50	I
3		29.09	6.09	I
	Average	29.19 ± 4.02	6.25 ± 0.84	
1	MB	20.02	5.58	I
2		23.31	6.50	I
3		31.18	8.70	I
	Average	24.84 ± 5.73	6.93 ± 1.60	
1	MC	16.88	7.06	I
2		21.46	8.98	I
3		8.27	3.46	I
	Average	15.54 ± 6.70	6.50 ± 2.80	
1	MD	6.24	5.22	I
2		6.64	5.56	I
3		6.01	5.03	I
	Average	6.30 ± 0.32	5.27 ± 0.27	
I : Interface Failure				

Table C Results for Measured Intrinsic Load and Intrinsic Interfacial Bond Strength

Trial	Specimen	Intrinsic Load (F_i) kN	Intrinsic Interfacial Bond Strength (τ_i) MPa
1	RLC	22.95	4.65
2		22.71	4.60
3		24.73	5.01
	Average	23.46 ± 3.36	4.75 ± 0.22
1	SLC	18.73	4.17
2		10.88	2.42
3		13.69	3.05
4		24.65	5.49
5		20.08	4.47
	Average	17.61± 4.85	3.92 ± 1.08
1	TLC	15.01	3.52
2		13.22	3.10
3		13.69	3.21
4		12.42	2.91
	Average	13.59 ± 1.08	3.19 ± 0.25
1	SC	21.57	5.68
2		21.60	5.69
	Average	21.58 ± 0.02	5.68 ± 0.01
1	MC	8.76	2.17
2		10.16	2.51
3		9.53	2.36
	Average	9.48 ± 0.70	2.34 ± 0.17
1	SC	3.98	1.12
2		4.56	1.29
3		2.74	0.77
4		3.06	0.86
		3.59 ± 0.84	1.01 ± 0.24

Table D Results for Measured Apparent Load and Apparent Interfacial Bond Strength

Trial	Specimen	Apparent Load (F_a) kN	Apparent Interfacial Bond Strength (τ_a) MPa
1	RLC	57.37	11.62
2		56.88	11.52
3	Average	57.13 ± 0.24	11.57 ± 0.05
1	SLC	50.29	11.20
2		36.99	8.24
3		37.69	8.39
4		43.73	9.74
5		43.96	9.79
	Average	42.53± 5.43	9.47 ± 1.21
1	TLC	34.77	8.15
2		28.89	6.77
3		37.69	8.84
	Average	13.59 ± 5.30	3.19 ± 0.25
1	SCC	56.34	14.83
2		72.24	19.02
3		54.65	14.39
4		39.49	10.40
		34.41	9.06
	Average	51.42 ± 15.00	13.53 ± 3.94
1	MC	27.2567	6.74
2		21.4266	5.30
3		21.9959	5.44
	Average	23.56 ± 3.21	5.82 ± 0.79
1	SC	4.96	1.40
2		4.89	1.38
3		3.66	1.03
4		3.53	1.00
	Average	4.26 ± 0.04	1.20 ± 0.21

Table E Results for Measured Frictional Resistance and Frictional Stress

Trial	Specimen	Frictional Resistance (F_f) kN	Frictional stress (τ_f) MPa
1	RLC	10.4024	2.571859
2		7.4871	1.851089
3	Average	8.94 ± 2.06	2.21 ± 0.51
1	SLC	9.23	2.28
2		8.52	2.11
3		7.15	1.77
	Average	8.30± 1.06	2.05 ± 0.26
1	TLC	6.39	1.58
2		6.83	1.69
	Average	6.61 ± 0.31	1.63 ± 0.08
1	SCC	12.9633	3.654774
2		19.6833	5.549359
	Average	16.32 ± 4.75	4.60 ± 1.34
1	MC	11.27	2.79
2		12.46	3.08
	Average	11.86 ± 0.85	2.93 ± 0.21
1	SC	0.97	0.27
2		0.33	0.09
3		0.92	0.26
4		0.47	0.13
	Average	0.67 ± 0.32	0.19 ± 0.09

Table F Results for Calculated Bearing Resistance

Trial	Specimen	Bearing Resistance (F_b) kN
1	RLC	24.02
2		26.69
	Average	25.36 ± 1.34
2	SLC	17.59
3		16.85
5		15.57
	Average	16.67 ± 1.02
1	TLC	13.37
2		8.84
3		14.59
	Average	12.27 ± 2.12
1	SCC	21.7953
2		13.3817
	Average	17.59 ± 4.21
1	MC	4.50
2		0.39
	Average	2.21 ± 2.91
1	SC	0.00
2		0.00
3		0.00
4		0.00
		0.00 ± 0.00

Table G Results for Measured Apparent Load with Three Different Loading Rate

Trial	Specimen	Loading rate	Apparent Load
1	SCC	6.5	56.2466
2			60.5963
		Average	58.42 ± 3.08
1		1.3	56.34
2			72.24
3			54.65
4			39.49
5			34.41
		Average	51.42 ± 15.08
1		0.26	40.1896
2			43.6172
		Average	41.90 ± 2.42
1	RLD	6.5	45.1093*
1		1.3	45.2017
2			41.2818
		Average	43.24 ± 2.77
1		0.26	55.0999
2			43.279
		Average	49.19 ± 8.36
* Note: Only one sample has been tested			

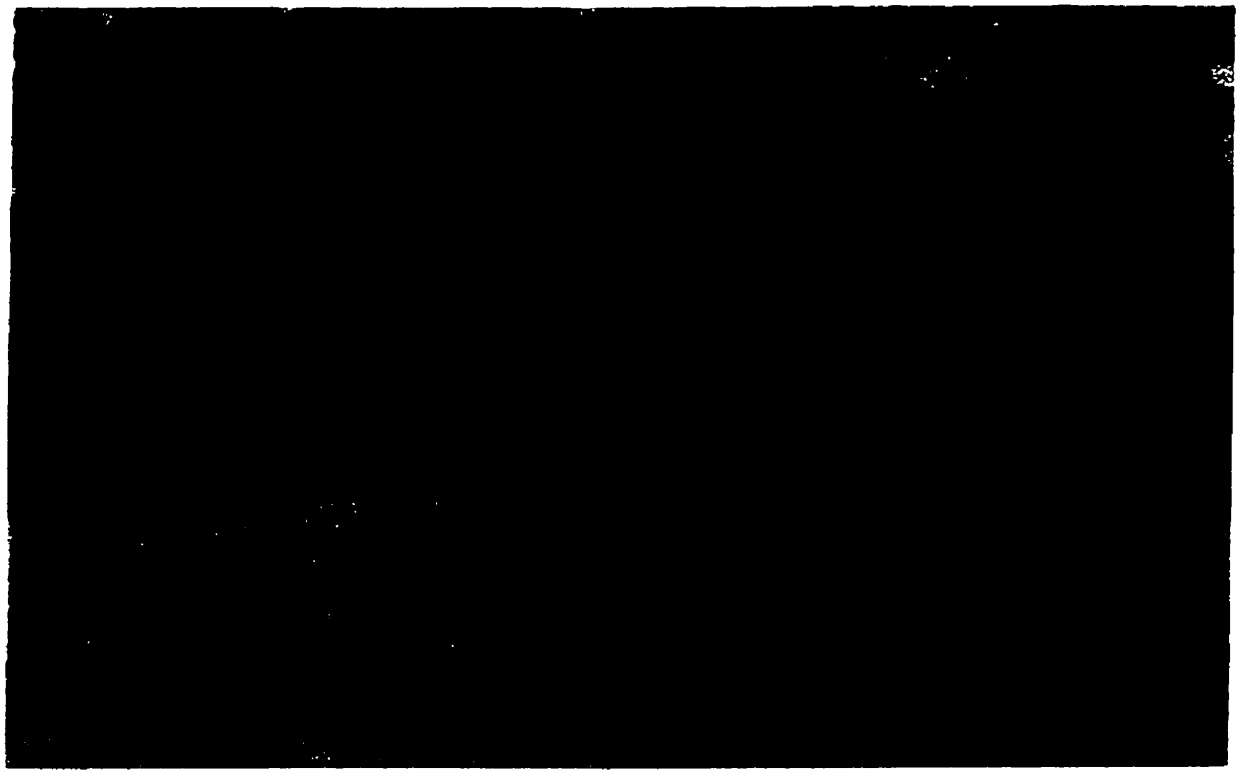

Figure A1 Post-mortem Examination on RLA specimen (F_a = 100%)

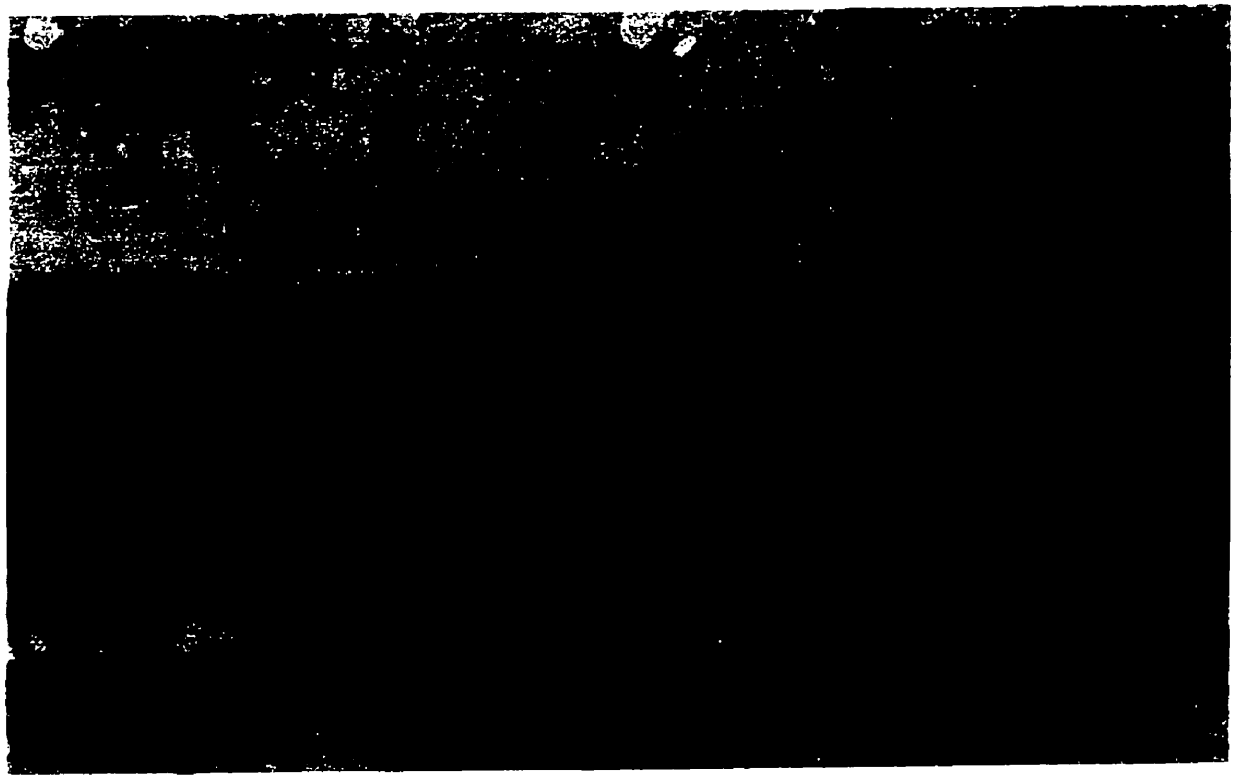

Figure A2 Post-mortem Examination on RLB specimen (F_a = 100%)

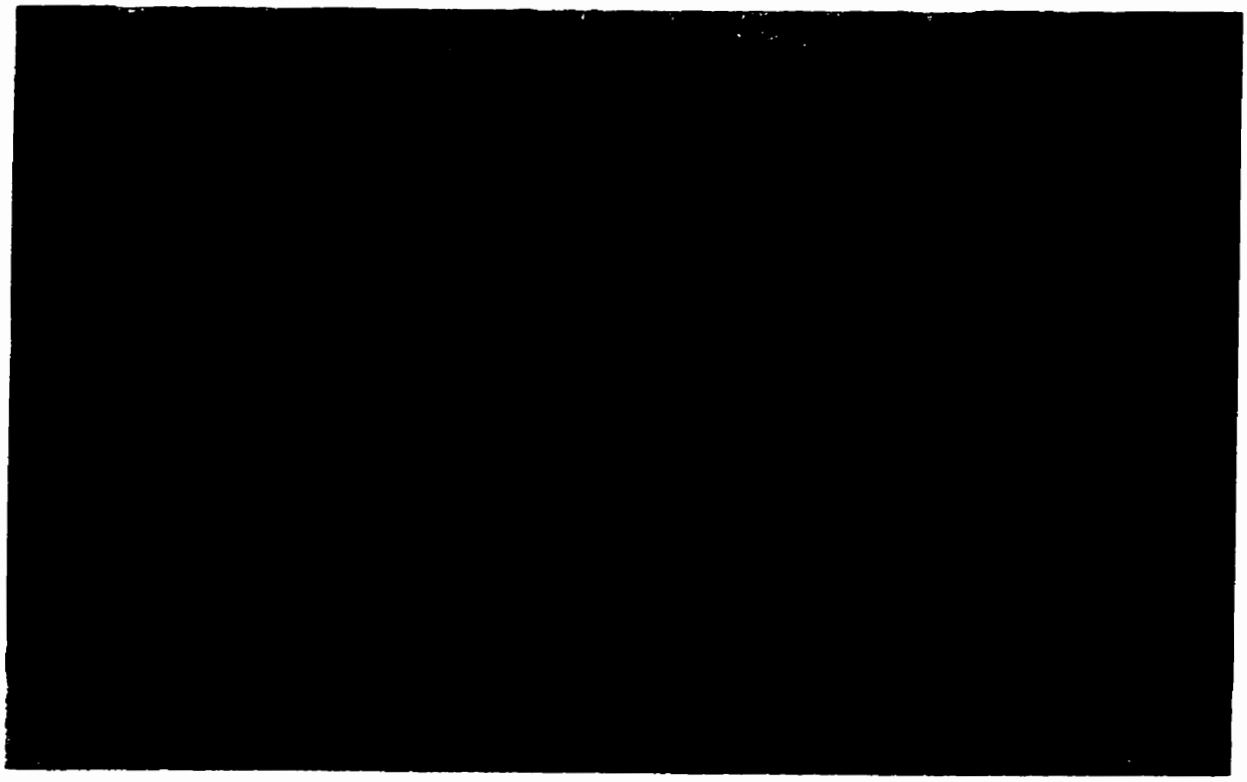

Figure A3 Post-mortem Examination on RLD specimen ($F_a = 100\%$)

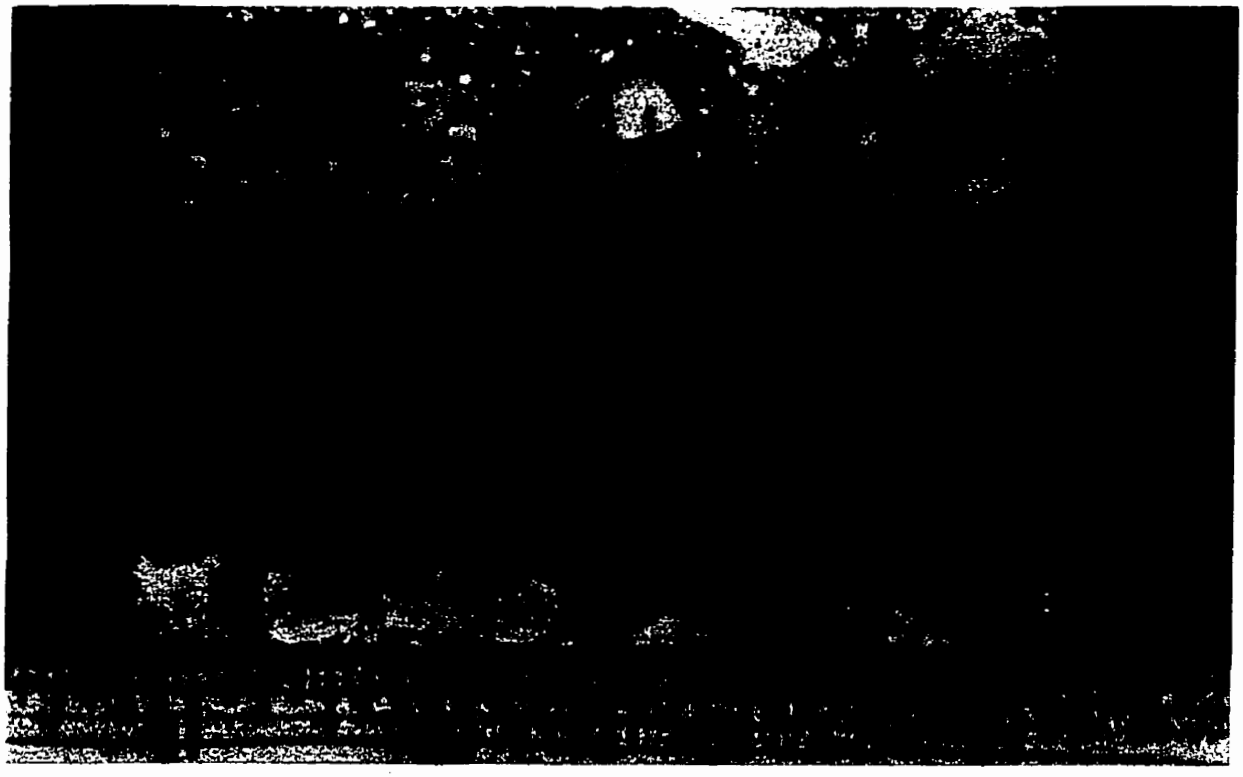

Figure A4 Post-mortem Examination on RLE specimen ($F_a = 100\%$)

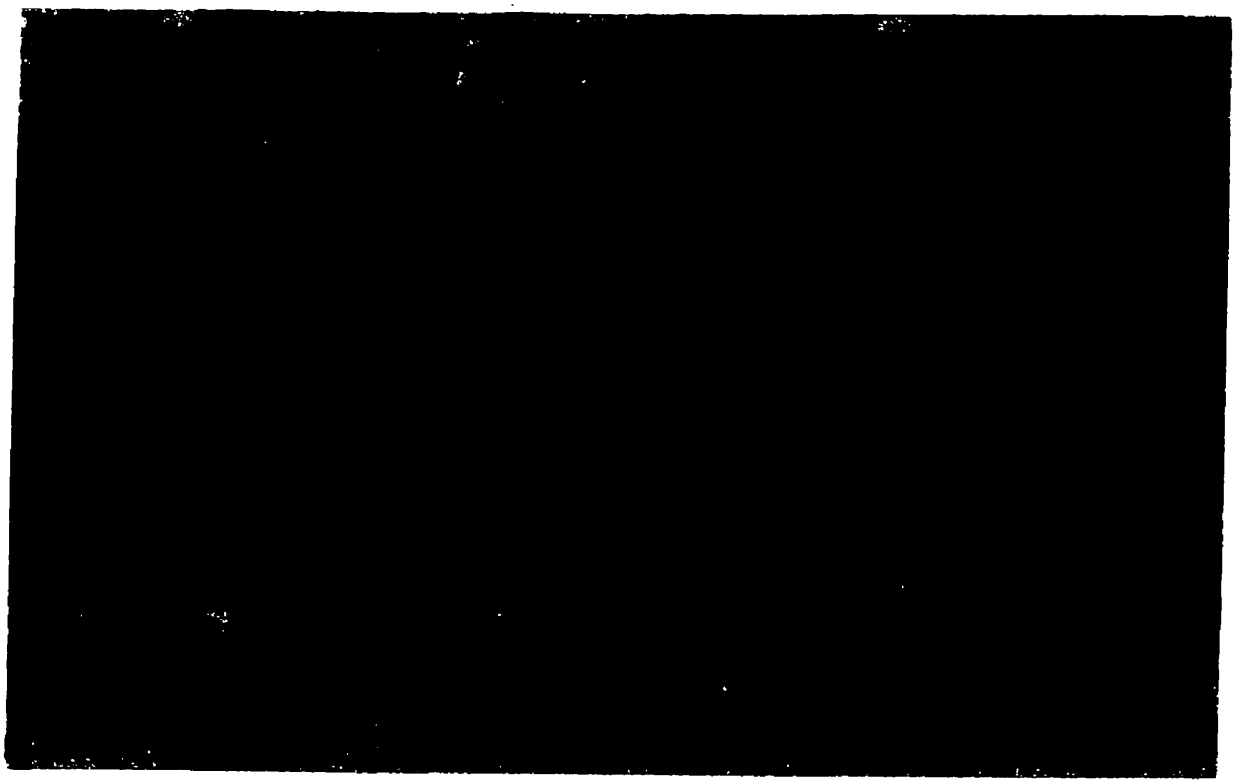

Figure B1 Post-mortem Examination on SCC specimen (F_a = 100%)

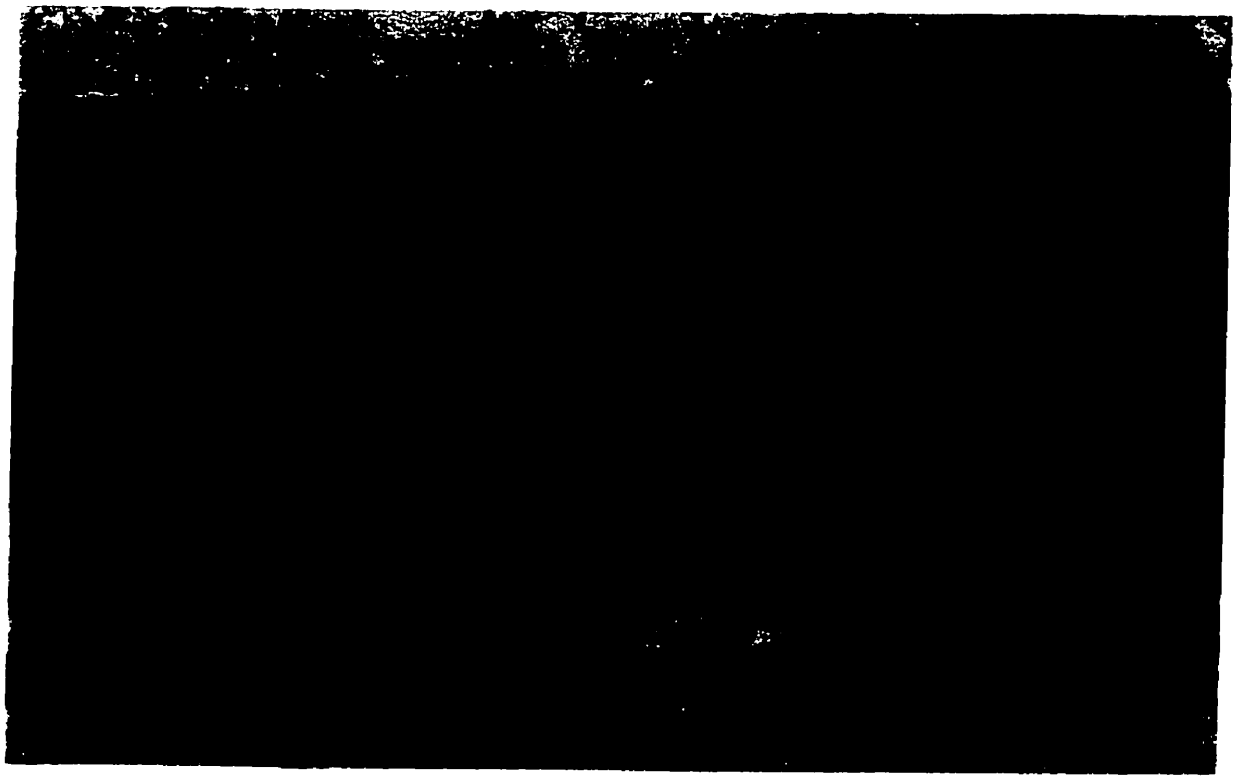

Figure B2 Post-mortem Examination on SCC specimen (F_a = 90%)

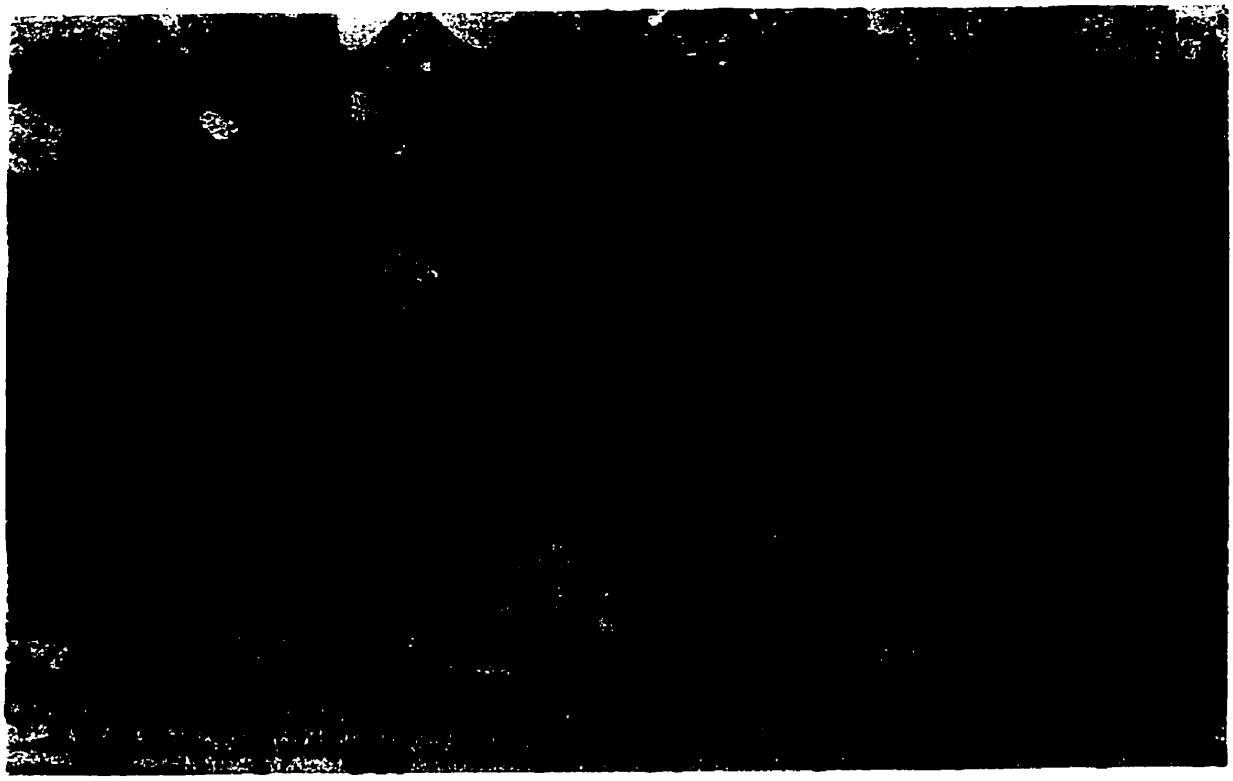

Figure B3 Post-mortem Examination on SCC specimen (F_a = 70%)

Figure B4 Post-mortem Examination on SCC specimen (F_a = 50%)

Figure C1 Post-mortem Examination on RLC specimen ($F_a = 85\%$)

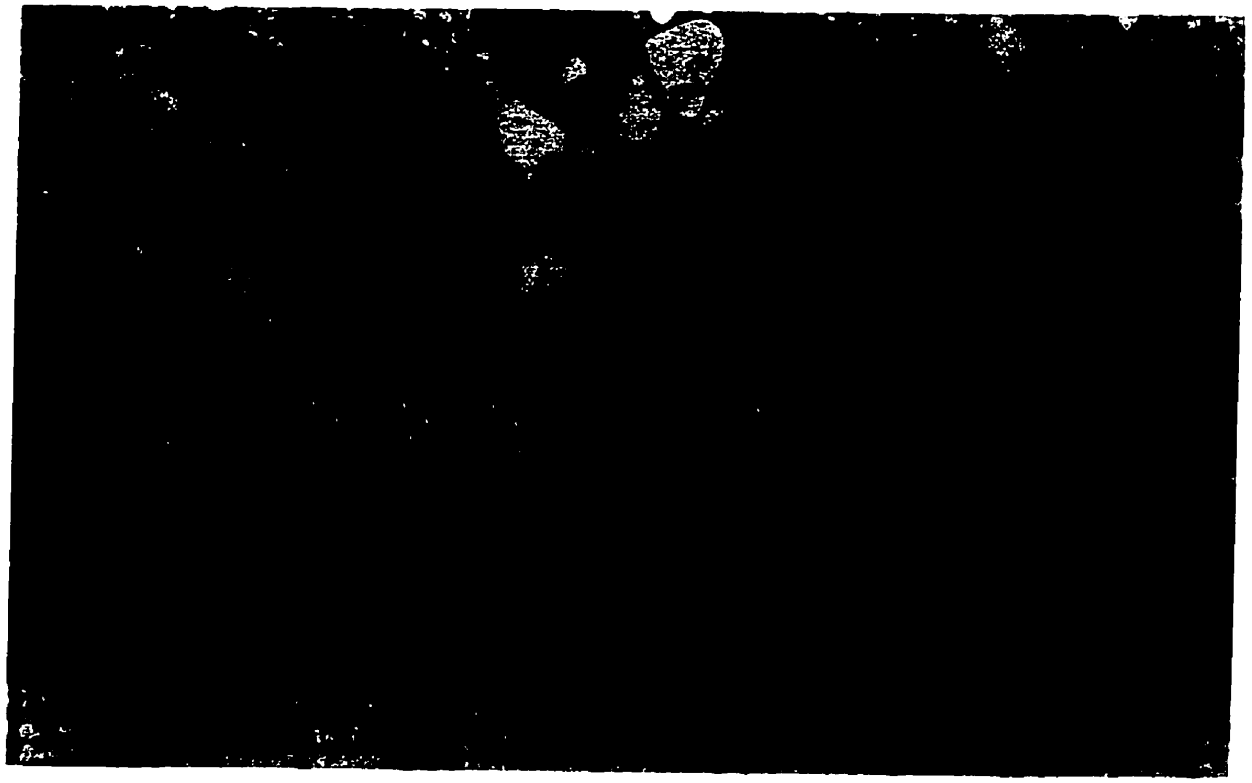

Figure C2 Post-mortem Examination on RLC specimen ($F_a = 60\%$)

Figure D1 Post-mortem Examination on SLC specimen (F_a = 100%)

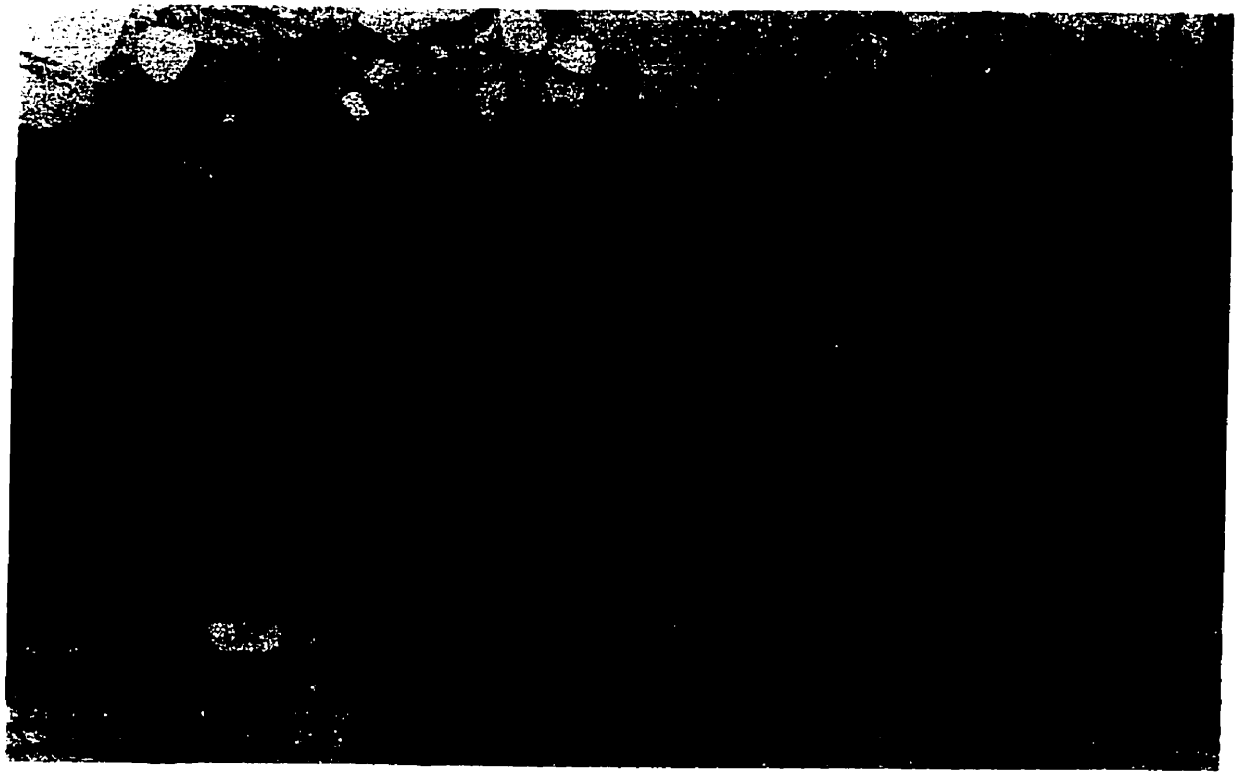

Figure D2 Post-mortem Examination on SLC specimen (F_a = 80%)

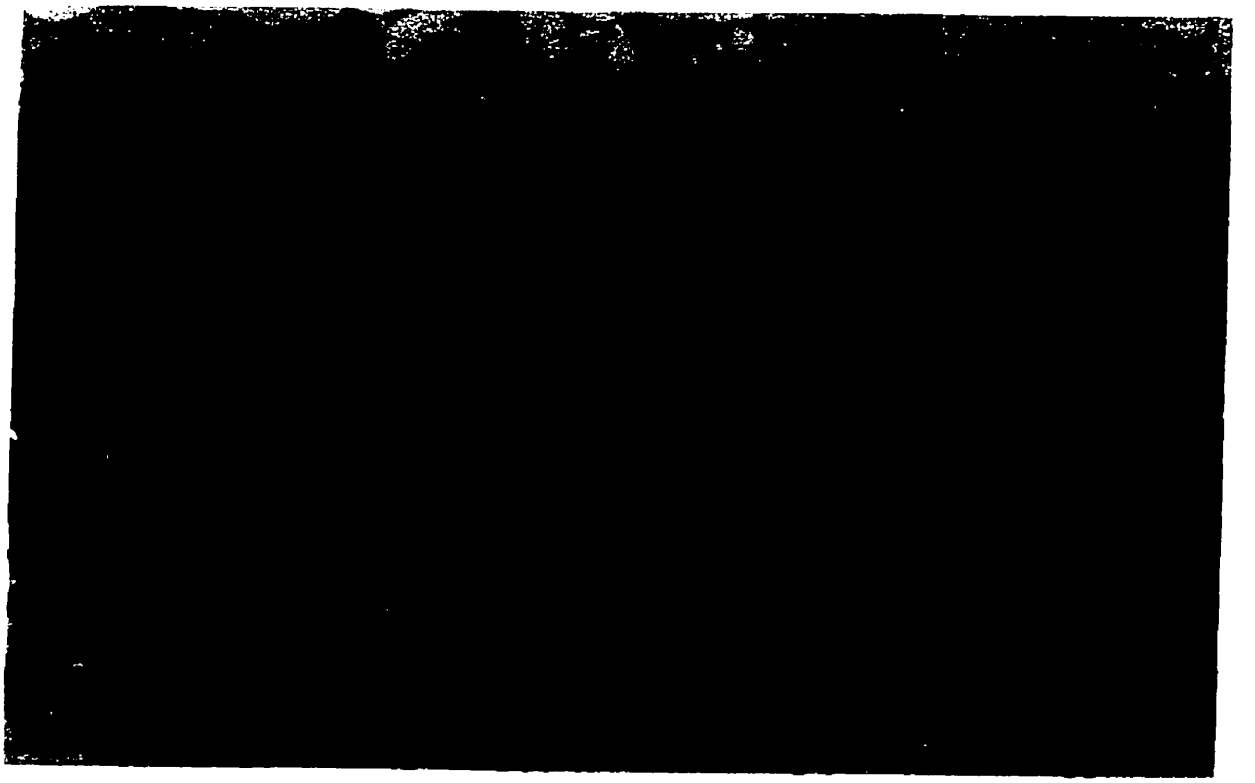

Figure D3 Post-mortem Examination on SLC specimen ($F_a = 60\%$)

Figure D4 Post-mortem Examination on SLC specimen ($F_a = 30\%$)

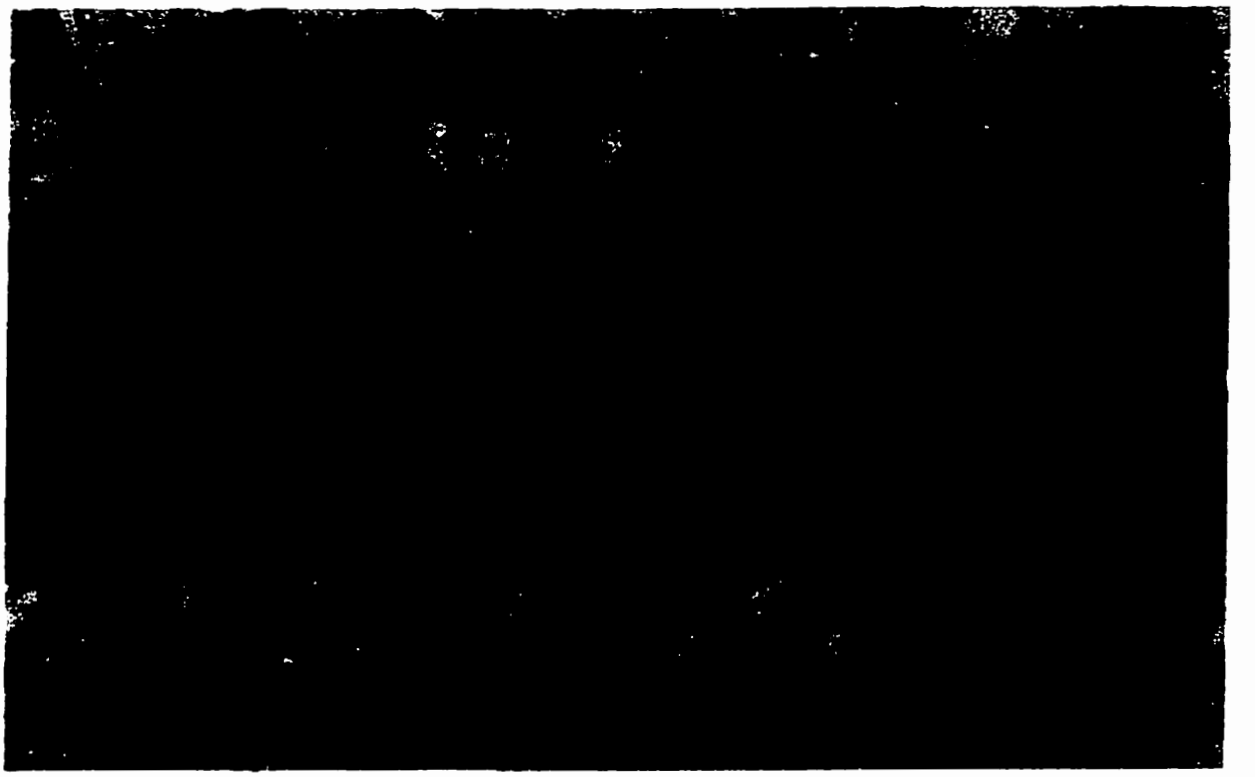

Figure E1 Post-mortem Examination on TLC specimen (F_a = 100%)

Figure E2 Post-mortem Examination on TLC specimen (F_a = 75%)